Activation, Permeability, and Inhibition of Astrocytic and Neuronal Large Pore (Hemi)channels

Hansen, Daniel Bloch; Ye, Zu-Cheng; Calloe, Kirstine; Braunstein, Thomas Hartig; Hofgaard, Johannes Pauli; Ransom, Bruce R.; Nielsen, Morten Schak; MacAulay, Nanna

Published in:
Journal of Biological Chemistry

Published: 19/09/2014

Document Version:
Final Published version, also known as Publisher's PDF, Publisher's Final version or Version of Record

Published version (DOI):
10.1074/jbc.M114.582155

Publication details:
Hansen, D. B., Ye, Z.-C., Calloe, K., Braunstein, T. H., Hofgaard, J. P., Ransom, B. R., Nielsen, M. S., & MacAulay, N. (2014). Activation, Permeability, and Inhibition of Astrocytic and Neuronal Large Pore (Hemi)channels. *Journal of Biological Chemistry*, *289*(38), 26058-26073. https://doi.org/10.1074/jbc.M114.582155

THE JOURNAL OF BIOLOGICAL CHEMISTRY VOL. 289, NO. 38, pp. 26058–26073, September 19, 2014

Activation, Permeability, and Inhibition of Astrocytic and Neuronal Large Pore (Hemi)channels*◆

Received for publication, May 19, 2014, and in revised form, July 25, 2014 Published, JBC Papers in Press, August 1, 2014, DOI 10.1074/jbc.M114.582155

Daniel Bloch Hansen[‡], Zu-Cheng Ye[§], Kirstine Calloe[¶], Thomas Hartig Braunstein[‖], Johannes Pauli Hofgaard[‖], Bruce R. Ransom[§], Morten Schak Nielsen[‖], and Nanna MacAulay[‡1]

From the [‡]Department of Cellular and Molecular Medicine, Faculty of Health and Medical Sciences, University of Copenhagen, 2200 Copenhagen N, Denmark, the [§]Department of Neurology, University of Washington, Seattle, Washington 98195, the [¶]Department of Veterinary Clinical and Animal Science, Faculty of Health and Medical Sciences, University of Copenhagen, 1870 Frederiksberg, Denmark, and the [‖]Danish National Research Foundation Centre for Cardiac Arrhythmia and Department of Biomedicine, Faculty of Health and Medical Sciences, University of Copenhagen, 2200 Copenhagen, Denmark

Background: The permeability and physiological role of several large pore (hemi)channels are unresolved.
Results: Large pore (hemi)channels, when heterologously expressed, display isoform-specific permeability and gating for ions and fluorescent dyes.
Conclusion: Large pore channels have isoform-specific transport characteristics that can be used for their identification.
Significance: Although large pore channels have characteristic properties in overexpression systems, these properties may be undetectable in native cells.

Astrocytes and neurons express several large pore (hemi)channels that may open in response to various stimuli, allowing fluorescent dyes, ions, and cytoplasmic molecules such as ATP and glutamate to permeate. Several of these large pore (hemi)channels have similar characteristics with regard to activation, permeability, and inhibitor sensitivity. Consequently, their behaviors and roles in astrocytic and neuronal (patho)physiology remain undefined. We took advantage of the *Xenopus laevis* expression system to determine the individual characteristics of several large pore channels in isolation. Expression of connexins Cx26, Cx30, Cx36, or Cx43, the pannexins Px1 or Px2, or the purinergic receptor $P2X_7$ yielded functional (hemi)channels with isoform-specific characteristics. Connexin hemichannels had distinct sensitivity to alterations of extracellular Ca^{2+} and their permeability to dyes and small atomic ions (conductance) were not proportional. Px1 and Px2 exhibited conductance at positive membrane potentials, but only Px1 displayed detectable fluorescent dye uptake. $P2X_7$, in the absence of Px1, was permeable to fluorescent dyes in an agonist-dependent manner. The large pore channels displayed overlapping sensitivity to the inhibitors Brilliant Blue, gadolinium, and carbenoxolone. These results demonstrated isoform-specific characteristics among the large pore membrane channels; an open (hemi)channel is not a nonselective channel. With these isoform-specific properties in mind, we characterized the divalent cation-sensitive permeation pathway in primary cultured astrocytes. We observed no activation of membrane conductance or Cx43-mediated dye uptake in astrocytes nor in Cx43-expressing C6 cells. Our data underscore that although Cx43-mediated transport is observed in overexpressing cell systems, such transport may not be detectable in native cells under comparable experimental conditions.

* This work was supported by the Danish Medical Research Foundation (to N. M.), and the Danish National Research Foundation (to M. S. N.).
◆ This article was selected as a Paper of the Week.
[1] To whom correspondence should be addressed: The Panum Institute, Blegdamsvej 3, Bldg. 12.6, 2200 Copenhagen N, Denmark. Tel.: 45-35327566; E-mail: macaulay@sund.ku.dk.

Neurons and glia cells express a variety of large pore channels, including connexins, pannexins, and purinergic ionotropic receptors (1–3). Connexins are the molecular building blocks of gap junctions, but select connexin isoforms have in recent years been demonstrated to function as transmembrane transport routes in their hemichannel configuration (4–8). A range of large pore (hemi)channels appears to open to the extracellular space in response to a variety of stimuli, such as removal of divalent cations from the extracellular solution, addition of receptor agonist, and/or at positive membrane potentials (4, 6, 8–10). Channel opening is commonly measured with various fluorescent dyes of molecular sizes ranging from ~300 to ~700 Da (9, 11, 12). Proportionality between dye uptake and permeability to biologically relevant molecules has, on occasion, been implied. However, the exact permeability profile for the majority of these channel types has not been determined.

Experimental determination of channel-specific characteristics may be obscured by the parallel expression of a range of large pore channels in the cell types of interest, their overlapping permeability profile, and their cross-sensitivity to commonly used inhibitors (13–17). Knock-out and knockdown strategies for several of the implicated large pore channels have been successfully applied to address this issue (9, 16, 18–20). However, interpretation of the findings is complicated by many uncontrolled factors, including protein-protein interactions, alternative splice variants, altered transcriptomes, and/or altered basal ATP concentrations, among others (9, 21–24), thus rendering the exact contribution of the different (hemi)-channels to dye uptake, ion conductance, and ATP/glutamate release unresolved.

Although several of these large pore channels serve as dye/ATP conduits as well as ion channels, some channels exhibit a noticeable disconnect between the ability to pass dyes/ATP and current; although dye uptake and ATP/glutamate/cAMP permeability can be detected at physiologically relevant membrane potentials in the negative range (4, 9, 27–29), membrane conductance for Px1 and Cx43 appears predominantly at positive membrane potentials (1, 4, 9, 25). Prolonged exposure to positive membrane potentials may even be required to detect Cx43-mediated membrane conductance (26). This seeming paradox may indicate that large pore channels do not act as nonselective freely diffusible pores but may, rather, possess the ability to selectively gate their permeability pathway (30).

Of the 21 different mammalian connexin isoforms (31), astrocytes express primarily Cx30 and Cx43 (and possibly Cx26), whereas Cx36 is the major neuronal connexin (3, 32–35). Connexins create gap junctional channels at cell to cell interfaces, allowing intercellular communication by transfer of current and small molecules (31). The permeability profile of gap junctional channels varies among isoforms (36); for example, Cx32 and Cx43 gap junctions have similar anionic/cationic current selectivity but orders of magnitude difference in their ATP/adenosine permeability (37). The molecular basis for these differences is unclear, although affinity between pore and permeant has been suggested for fluorescent dyes (38). Although connexins 26, 30, 36, and 43 are all deemed functional in their hemichannel configuration (6–8, 29), their isoform-specific sensitivity to extracellular Ca^{2+}, dye permeability, conductance, and inhibitor sensitivity as hemichannels remain to be established.

Activation of the purinergic receptor, $P2X_7$, initially results in increased membrane conductance, whereas sustained activation induces formation of a pore also permeable to fluorescent dyes and large cytosolic molecules (10, 39). The large pore is either formed by $P2X_7$ itself in a process termed pore dilation (10, 40, 41) or alternatively, as a result of recruitment and activation of Px1 (42–44). Whether Px1-$P2X_7$ interaction is required to induce the large pore thus remains controversial.

In this study, we expressed the neuronal and astrocytic large pore (hemi)channels (*i.e.* Cx26, Cx30, Cx43, Cx36, Px1, Px2, $P2X_7$, and Px1/$P2X_7$ co-expression) in *Xenopus laevis* oocytes, a heterologous expression system that allows for biophysical characterization of channel properties in an isolated setting. We were thus able to elucidate select isoform-specific channel characteristics, activation regimes, and inhibitor profiles of this subset of large pore channels. Finally, we employed primary cultured astrocytes and Cx43-expressing C6 cells to determine the quantitative contribution of Cx43 hemichannels in divalent cation-free solution (DCFS)[2]-induced dye uptake and membrane conductance in a physiologically relevant setting.

EXPERIMENTAL PROCEDURES

Heterologous Expression in X. laevis Oocytes—Oocytes were surgically removed from *X. laevis* frogs (Nasco or National Center for Scientific Research, France) in accordance with The Danish National Committee for Animal Studies under the Ministry of Justice. Stage V–VI oocytes were defolliculated and isolated as described previously (45) followed by incubation in Kulori medium containing (in mM) 90 NaCl, 1 KCl, 1 $MgCl_2$, 1 $CaCl_2$, 5 HEPES, pH 7.4, at 18 °C for up to 24 h prior to cRNA injection. cDNA encoding hCx26 (obtained from Thomas W. White, Stony Brook University, New York), mCx30 and mCx36 (obtained from Klaus Willecke, Bonn University), rCx43 (obtained from Zealand Pharma, Denmark), $hP2X_7$ (obtained from Gunter Schmalzing, University of Kaachen via Rainer Schreiber, University of Regensburg, Germany), and rPx1 and rPx2 (obtained from Robert Bruzzone via Gina Sosinsky, University of California at San Diego School of Medicine (46)) were subcloned into the expression vector pXOOM optimized for oocyte expression by addition of untranslated RNA-stabilizing elements (47). The coding sequence of the cDNA was verified by sequencing prior to linearization downstream from the poly(A) segments. The cDNA was *in vitro* transcribed to cRNA with mMessage mMachine T7 (Ambion, Denmark) followed by transcript purification with MEGAclear (Ambion, Denmark). Oocytes were injected with 10 ng of cRNA using a Nanoject microinjector (Drummond Scientific, PA) and kept in Kulori medium at 18 °C for 3–6 days prior to experiments. We have previously demonstrated that the endogenous *Xenopus* Cx38 does not contribute to DCFS-induced dye uptake and membrane current in our hands (30). Cx38 antisense has therefore not been co-injected in this study.

Cell Cultures—Cortical astrocytes were prepared from neonatal or P7 rat pups (Sprague-Dawley) or neonatal mouse pups ($Cx43^{-/-}$ (glia-specific KO, provided by Ken McCarthy; B6;129 (48)) with wild-type (WT) C57BL/6 as control). The $Cx43^{-/-}$ mice displayed no Cx43 expression in hippocampal tissue or cultures as detected by immunohistochemistry and Western blotting, and no compensatory changes in Cx30 expression were detected (16). Briefly, meningeal tissue was removed and the neocortex minced by pipetting, and the dissociated cells were plated on glass coverslips with culture medium consisting of Earle's minimum essential media (Invitrogen) supplemented with 10% fetal bovine serum (HyClone, Logan, UT), 20 mM glucose, 10 units/ml penicillin, and 10 μg/ml streptomycin. Culture medium was changed every 3–4 days. Cells were used after 1–4 weeks in culture.

Native C6 glioma cells and C6 glioma cells transduced with Cx43 (C6 Cx43) were kindly provided by Zealand Pharma, Denmark. Cells were plated at low density on glass coverslips and incubated in Dulbecco's modified Eagle's medium (DMEM) containing 10% fetal bovine serum (FBS), 100 units/ml penicillin, and 100 μg/ml streptomycin at 37 °C with 5% CO_2 and used after 1–3 days in culture.

Electrophysiology—*X. laevis* oocytes were continuously superfused with NaCl solution (containing in mM: 100 NaCl, 2 KCl, 1 $CaCl_2$, 1 $MgCl_2$, 10 HEPES, 4 Tris ($(HOCH_2)_3CNH_2$), pH 7.4, at room temperature) or NaCl solution without divalent cations (DCFS) in which Ca^{2+} and Mg^{2+} salts were substituted with equiosmolar NaCl with or without 30 μM BzATP (see under "Chemicals") as indicated in the figure legends. The solution change took place with a custom-made continuous

[2] The abbreviations used are: DCFS, divalent cation-free solution; ANOVA, analysis of variance; BzATP, 2′(3′)-*O*-(4-benzoylbenzoyl)ATP; a.u., arbitrary unit; Cx, connexin; h, human; r, rat; m, mouse; pF, picofarad.

flow system. Although trace amounts of divalent cations are likely to be present in the DCFS solution, we estimate this concentration to be below 3 μM during the experimental condition based on trace amounts in the chemicals present in the test solution, glassware, and the weak Ca^{2+}-chelating properties of Tris($(HOCH_2)_3CNH_2$). Borosilicate glass capillary electrodes were pulled to a resistance of 1–2 megohms when filled with 1 M KCl. Currents were recorded from a holding potential of −50 mV by application of 100-ms voltage steps from −140 to +60 mV or 10-s voltage steps from −60 to +60 mV in intervals of 20 mV following 1 min of exposure to experimental solution, and *I*/*V* relations were obtained from the steady-state current levels. The recordings were performed with a Dagan Clampator interfaced to a PC with a Digidata 1320 A/D converter and pClamp 9.2 (Both Axon Instruments, CA). Currents were low pass-filtered at 500 Hz and sampled at 2 kHz.

Cultured astrocytes were seeded on coverslips that were mounted on the stage of an inverted microscope (Zeiss Axiovert S10). The cells were superfused at 1 ml/min with NaCl solution (containing in mM: 124 NaCl, 3 KCl, 1 $MgCl_2$, 1.8 $CaCl_2$, 5 D-glucose, 20 HEPES, pH 7.4, 37 °C) or similar solution without divalent cations (DCFS, equiosmolar substitution with NaCl). The solution change took place with continuous superfusion. Patch pipettes were pulled from borosilicate capillaries (GC150F, Harvard Apparatus, Edenbridge, UK) to a resistance of 4–6 megohms. The pipettes were front-loaded with pipette solution (containing in mM: 70 K_2SO_4, 10 NaCl, 1 $CaCl_2$, 1 $MgCl_2$, 10 HEPES, pH 7.2) and subsequently back-filled with the same pipette solution including 0.26 mM amphotericin B (Sigma) for perforated patch clamping (49). A gigaohm seal was created on single cells, and the reduction in access resistance, due to amphotericin B generating monovalent ion-permeable pores in the membrane, was monitored as changes in the capacitive transients. A plateau in access resistance was obtained after 7–8 min, and currents were recorded from a holding potential of −80 mV by application of 1-s voltage steps from −100 to +60 mV in intervals of 20 mV; *I*/*V* relations were obtained from the steady-state current levels. The recordings were performed with an EPC7 amplifier (Heka, Germany), a Digidata 1440B A/D converter, and PClamp10 software (both from Axon Instruments). Currents were filtered at 3 kHz and sampled at 10 kHz.

Dye Uptake—Five oocytes were washed in the respective test solution and subsequently transferred to the dye-containing test solution by a custom-made Pasteur pipette in which the oocytes were surrounded by the wash solution. The experiment was carried out in the well of a 24-well cell culture plate containing 0.5 ml of experimental solution, either NaCl solution or NaCl DCFS (described above) with or without 10 μM BzATP as indicated in the legends. The test solution contained 50 μM ethidium bromide, 10 μM Yo-Pro, 50 μM propidium iodide, or 50 μM carboxyfluorescein (see under "Chemicals"), and the uptake was performed with mild agitation for 1 h at room temperature. The oocytes were subsequently swiftly washed three times in 1 ml of NaCl control solution and placed individually in the wells of a 96-well microtiter plate and lysed in 50 μl of water (Milli-Q) by repeated pipetting. Dye content of each well was determined with a Synergy HD plate reader and Gen5 software (both from BioTek) with the following filters for excitation and emission: 340/11 and 590/35 nm for ethidium, 530/25 and 635/32 nm for propidium iodide, and 485/20 and 528/20 nm filters for Yo-Pro and carboxyfluorescein. Background fluorescence averaged from two untreated oocytes was subtracted before data analysis.

Astrocytes were cultured on coverslips that were mounted in a heated closed chamber (TC-344B, Warner Instruments) on an inverted microscope (Leica DMI6000 B) with a 40 × 1.25–0.75 NA HCX PL APO oil objective (both Leica Microsystems, Wetzlar, Germany) and kept at 37 °C with an objective heater system (Bioptics). Fluorescence was sampled at 20-s intervals and recorded with MetaFluor software (Metafluor 7.6.2.0, Molecular Devices). A region of interest covering the full frame was chosen due to astrocytic morphological changes following removal of divalent cations. Dye uptake was measured using a monochromator (Polychrome V, TILL Photonics, Germany) exciting at 450 nm for ethidium and 490 nm for Yo-Pro, and emission was measured with filters allowing passage of wavelengths >510 nm (Leica Microsystems, Wetzlar, Germany). Cells were superfused at 0.5 ml/min with NaCl solution (containing in mM: 126 NaCl, 3 KCl, 1.25 NaH_2PO_4, 2 $CaCl_2$, 2 $MgCl_2$, 25 HEPES, 10 glucose, 10 $MgSO_4$, 0.25 μM Yo-Pro, and/or 1 μM ethidium bromide, pH 7.4, 37 °C) followed by a solution change via continuous superfusion to DCFS (Ca^{2+} and Mg^{2+} substituted by equiosmolar NaCl). Linear regression analysis was performed on the uptake during the last 5 min (out of 10 min) in each solution, and slopes were normalized to those obtained in control solution.

C6 cells were plated at low density on glass coverslips. The coverslips were mounted in a chamber on the stage of an inverted microscope (Zeiss Axiovert S100) with a 40× 1.3 NA FLUAR oil objective (Carl Zeiss Micro Imaging GmbH, Jena, Germany). No morphological changes in C6 cells were observed following removal of divalent cations, and regions of interest were placed randomly over single cells, with a minimum of five cells chosen per experiment. Fluorescence was sampled at 10-s intervals and recorded with MetaFluor software (Metafluor 7.6.2.0, Molecular Devices). Ethidium uptake was measured using a monochromator (Polychrome V, TILL Photonics) exciting at 340 nm and a filter allowing passage of wavelengths >520 nm for emission. Cells were superfused at 0.7 ml/min with NaCl solution (containing in mM: 124 NaCl, 3 KCl, 1.8 $CaCl_2$, 1 $MgCl_2$, 5 D-glucose, 20 HEPES, and 50 μM ethidium bromide, pH 7.4, room temperature), followed by a solution change via continuous superfusion to DCFS and finally in NaCl-EDTA (Ca^{2+} and Mg^{2+} substituted by 2 mM EDTA).

Immunocytochemistry—For immunocytochemistry, monolayers of C6 cells (native or C6 Cx43) were fixed in 3% paraformaldehyde. The cells were permeabilized, and immunocytochemistry was performed with a polyclonal anti-Cx43 antibody, 1:1000 (C6219, Sigma), and a secondary Alexa 488-conjugated antibody followed by counterstaining with phalloidin conjugated to Alexa 555 (both Invitrogen). Cells were imaged in a laser scanning microscope (Zeiss LSM 780) with a 63× 1.4 NA oil objective (Carl Zeiss MicroImaging GmbH, Jena, Germany).

Statistics and Data Analysis—All oocyte uptake experiments were repeated at least three times, each with oocytes from dif-

ferent animal donors and each with five oocytes per condition. Dye uptake in cultured rat and mouse primary culture of astrocytes was carried out with three different astrocytic preparations. All experiments on wild-type and Cx43 knock-out mouse astrocytes were performed in parallel (same days, same solutions, and same number of days in culture). Dye uptake in C6 cells was carried out on three distinct batches. *n* for uptake in oocytes, astrocytes, or C6 indicates the number of experiments, and *n* for electrophysiology indicates the number of individual oocytes/astrocytes.

Best fit was determined by the extra sum-of-squares *F* test, and three- or four-parameter logistic nonlinear regression analysis was performed with Prism 6.02 (GraphPad Software) on the Ca^{2+}- or inhibitor-sensitive component of ethidium uptake or current using Equations 1 and 2,

$$Y = \text{min} + (100\% - \text{min})/(1 + 10\text{^}(X - \text{log}IC_{50})) \quad \text{(Eq. 1)}$$

$$Y = \text{min} + (100\% - \text{min})/(1 + 10\text{^}((\text{log}IC_{50} - X) \cdot \text{Hill slope})) \quad \text{(Eq. 2)}$$

Astrocytic and C6 dye uptake was analyzed with linear regression and normalized to uptake obtained in control solution. Fluorescence is given as arbitrary units (a.u.). Statistical analysis was performed with Prism 6.02, using *t* test or ANOVA with Holm-Šídák multiple comparison post hoc test. Because equal variances are a prerequisite for using ANOVA, we used Kruskal-Wallis with Dunn's post hoc test in cases where between groups variance differed significantly as determined by the Brown-Forsythe test. Regression analysis and statistical tests are indicated in legends. $p < 0.05$ was considered significant. Values in text are given as average ± S.E.

Chemicals—Inhibitors and fluorescent dyes from Sigma were prepared as follows: $GdCl_3$ (H_2O, 100 mM), BzATP (H_2O, 3 mM, prepared freshly every 2nd week and stored at 5 °C), Brilliant Blue G (H_2O, 50 mM), carbenoxolone (H_2O, 100 mM, prepared freshly every 2nd week and stored at 5 °C), ethidium bromide (H_2O, 25 mM), Yo-Pro (DMSO, 1 mM), propidium iodide (H_2O, 1 mM), carboxyfluorescein (H_2O, 10 mM). DMEM, FBS, penicillin, and streptomycin were from Invitrogen.

RESULTS

Dye Permeability and Conductance of Connexin-expressing Oocytes—To determine the isoform-specific permeability characteristics of connexins Cx26, Cx30, Cx36, and Cx43, these constructs were expressed in *X. laevis* oocytes. As an initial measure of connexin hemichannel opening, we determined the uptake of the fluorescent molecule ethidium (314 Da) into individual connexin-expressing oocytes.

In control solution containing divalent cations (1 mM of each), the ethidium uptake observed in Cx26- and Cx30-expressing oocytes was not significantly different from that of the uninjected oocytes (Fig. 1*a*, *white bars*), indicating no basal hemichannel activity by these connexin isoforms. In contrast, Cx36- and Cx43-expressing oocytes displayed a significantly higher ethidium uptake than the uninjected oocytes (341 ± 45 and 207 ± 20 *versus* 111 ± 12 a.u., $n = 5–7$, $p < 0.05$) in a gadolinium-sensitive manner (50 μM, Fig. 1*a*, *hatched bars*). Removal of divalent cations (*i.e.* Mg^{2+} and Ca^{2+}) can induce connexin hemichannel opening (6, 8, 11, 29), and we, accordingly, exposed oocytes to DCFS (Fig. 1*a*, *gray bars*). The ethidium uptake of uninjected oocytes was insensitive to removal of divalent cations (111 ± 20 *versus* 101 ± 5 a.u., $n = 7$), whereas DCFS induced a significant increase in ethidium uptake in Cx30- and Cx43-expressing oocytes (557 ± 108 *versus* 142 ± 5 and 432 ± 57 *versus* 207 ± 20 a.u., respectively, $n = 5–6$, $p < 0.001$ and 0.05, *gray bars*) in a gadolinium-sensitive manner (Fig. 1*a*, *gray hatched bars*). Exposure to DCFS had no significant effect on ethidium uptake in Cx26- or Cx36-expressing oocytes compared with control solution ($p > 0.4$).

The Ca^{2+} sensitivity of the DCFS-activated Cx30 hemichannel was determined in the absence of Mg^{2+}. Cx30-expressing oocytes were exposed to increasing concentrations of extracellular Ca^{2+}, and the hemichannel activity was determined as the Cx-mediated ethidium uptake following subtraction of the contribution from the uninjected oocyte. The Cx30 IC_{50} value for Ca^{2+} was similar to that of Cx43 (44 ± 6 μM for Cx30 and 30 ± 9 μM for Cx43 (30), $n = 5–6$), although the Hill coefficient (slope) was steeper for Cx30 than for Cx43 (the Ca^{2+} sensitivity for Cx43-mediated dye uptake (Fig. 1*b*, *dashed line*) was adapted from Ref. 30)). Cx30-mediated hemichannel activity was fully inhibited by 0.5 mM Ca^{2+} (Fig. 1*b*), whereas Cx43-mediated hemichannel activity reached its minimum at 2 mM Ca^{2+} (30).

To further probe for connexin isoform-specific differences, we determined the hemichannel-mediated permeability toward another commonly used fluorescent probe, Yo-Pro (375 Da). The experiments were carried out in DCFS. Cx-mediated Gd^{3+}-sensitive Yo-Pro uptake was observed exclusively in Cx30-expressing oocytes (13,815 ± 5759 *versus* 3820 ± 996 a.u. in uninjected oocytes, $n = 7$ and 12, $p < 0.01$, Fig. 1*c*), whereas no significant uptake was observed in oocytes expressing the other tested isoforms. A similar pattern was observed with propidium iodide (668 Da) (data not shown). These data illustrate that dye uptake via Cx hemichannels displays isoform-specific characteristics regarding both Ca^{2+} sensitivity and dye selectivity.

To determine whether hemichannel-mediated dye permeability was paralleled by ionic conductance, we applied two-electrode voltage clamp to connexin-expressing oocytes (Fig. 2). In control solution, the membrane current for Cx26- and Cx30-expressing oocytes was slightly increased compared with that of uninjected oocytes (250 ± 40 and 316 ± 33 nA *versus* 143 ± 8 nA at +60 mV, $n = 15$, 10, and 19, $p < 0.05$), whereas the membrane current for Cx36- and Cx43-expressing oocytes was comparable with the uninjected control (137 ± 8, 168 ± 9, and 143 ± 8 nA at +60 mV, $n = 8–19$). Exposure to DCFS (1 min) induced large Cx-mediated membrane currents in oocytes expressing Cx26 and Cx30 (2041 ± 415 and 2390 ± 631 nA at +60 mV, $n = 15$ and 10, $p < 0.01$ compared with uninjected oocytes; 317 ± 32 nA, $n = 19$), whereas the DCFS-induced membrane current for Cx36- and Cx43-expressing oocytes was similar to that of the uninjected control oocytes. Applying a longer pulse of 10 s to Cx43-expressing oocytes also failed to

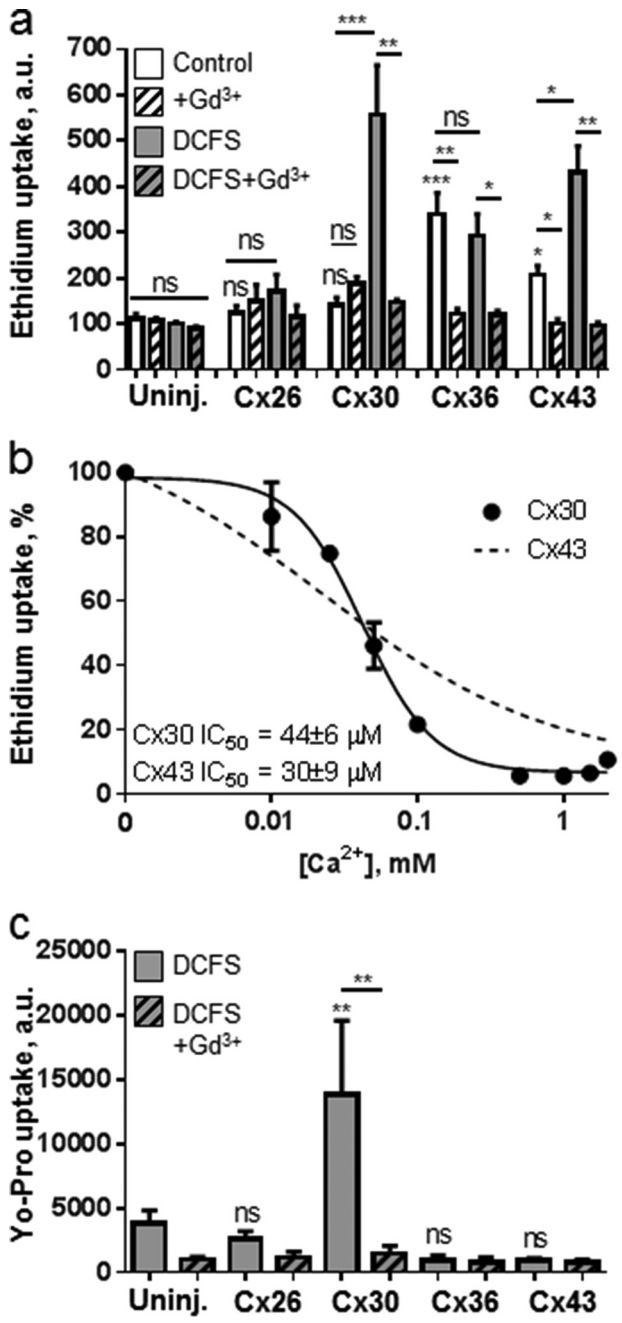

FIGURE 1. **Differences in hemichannel-mediated ethidium and Yo-Pro uptake following removal of divalent cations.** *a,* dye uptake in uninjected and connexin-expressing oocytes in control solution containing 1 mM Ca^{2+} and Mg^{2+} (*white bars*), in divalent cation-free solution without Ca^{2+} and Mg^{2+} (DCFS, *gray bars*), and without or with 50 μM Gd^{3+} (*hatched bars*). Values are given in arbitrary units (*a.u.*), $n = 4–6$ experiments. Statistical significance between ethidium uptake in uninjected and all connexin-expressing oocytes in control solution (significance indicated directly over the relevant bar in the diagram) and within-group comparisons for uninjected, Cx26-, Cx36-, and Cx43-expressing oocytes (significance provided over lines indicating the given comparison) were performed using ANOVA with Holm-Šídák post hoc test, whereas the within-group comparisons of Cx30-expressing oocytes were performed using Kruskal-Wallis with Dunn's post hoc test. *b,* ethidium uptake was determined in Cx30-expressing oocytes in test solutions without Mg^{2+} and with Ca^{2+}-concentrations from 0 to 2 mM. Uninjected oocyte background uptake was subtracted, and the Cx30-mediated ethidium uptake was normalized to uptake obtained in DCFS followed by three-parameter nonlinear regression analysis. Each data point averages five experiments; the *line* indicates best fit, and IC_{50} was determined as the average of five independent regression analyses. Calcium sensitivity for Cx43 is included for comparison (*dashed line*) (30). *c,* Yo-Pro uptake in uninjected (*Uninj.*) and connexin-expressing oocytes in DCFS in the absence (*gray bars*) or presence of 50 μM Gd^{3+} (*hatched bars*). Values are given in arbitrary units. $n = 3–12$ experiments, and statistical significance was determined using one-way ANOVA with Holm-Šídák post hoc test and illustrated as in *a*. *Error bars* indicate S.E. *ns,* not significant, *, $p < 0.05$; **, $p < 0.01$; ***, $p < 0.001$.

activate a conductance, and the current in DCFS was similar to that of the uninjected oocytes (455 ± 155 *versus* 385 ± 150 nA at +60 mV, $n = 7$, $p > 0.7$). The permeation pathway through connexin hemichannels, when expressed in *Xenopus* oocytes, appears to be highly selective toward fluorescent dyes and/or ions. The different connexins thus display distinct isoform-specific behavior in their hemichannel configuration.

Dye Permeability and Conductance of Pannexin-expressing Oocytes—Pannexins constitute another group of large pore channels and may have some functionality in common with the connexin hemichannels. We determined the dye permeability and membrane conductance in oocytes expressing two pannexin isoforms, Px1 or Px2. Px1- and Px2-expressing oocytes displayed an outwardly rectifying membrane conductance at positive membrane potentials although smaller for Px2-expressing oocytes than for Px1-expressing oocytes (1130 ± 61, 365 ± 39, and 133 ± 10 nA at +60 mV for Px1, Px2, and uninjected, respectively, $p < 0.001$, $n = 9–17$) (Fig. 3*a*).

In control solution, Px1-expressing oocytes displayed greater uptake of ethidium and Yo-Pro than the uninjected oocytes (Fig. 3, *b* and *c*, *white bars*). The ethidium and Yo-Pro uptake of Px2-expressing oocytes was similar to those obtained in the uninjected oocytes, illustrating no detectable ethidium and Yo-Pro permeability through Px2 (Fig. 3, *b* and *c*). Exposure to DCFS had no effect on ethidium uptake in Px1- or Px2-expressing oocytes (Fig. 3*b*, *gray bars*). We found a tendency, although it did not reach statistical significance, toward carboxyfluorescein permeability through Px1 (766 ± 122 a.u., $n = 6$, $p > 0.27$) and Px2 (981 ± 304 a.u., $n = 5$, $p > 0.15$) as compared with that of the uninjected oocytes (469 ± 130 a.u., $n = 6$) (Fig. 3*d*). Exposure to the $P2X_7$ agonist BzATP (10 μM, see below) did not affect dye uptake in Px1- or Px2-expressing oocytes (data not shown). Thus, Px1 displayed permeability to ethidium and Yo-Pro in a nongated manner at resting membrane potential, whereas Px1-mediated ion conductance was observed only at positive membrane potentials.

Dye Permeability and Conductance of $P2X_7$-expressing Oocytes—To determine whether the purinergic receptor $P2X_7$ possesses the inherent ability to allow dye permeation (*versus* the proposed requirement for Px1 (42, 44)), we determined the permeability and activation profile for $P2X_7$-expressing oocytes. In control solution, as well as in DCFS, $P2X_7$-expressing oocytes displayed membrane conductance similar to that of the uninjected oocytes (compare Fig. 4*a* ($P2X_7$) and 3*a* (*Uninj.*)). Addition of the $P2X_7$ agonist BzATP (30 μM) to the test solution induced a large, nonrectifying, and fully reversible membrane conductance (Fig. 4*a, inset*). Note that the current pattern induced by BzATP was biphasic, with an initial "shoulder" (Fig. 4*a*, *inset*). BzATP-induced current was not observed in uninjected oocytes (data not shown).

In control solution, the dye uptake of $P2X_7$-expressing oocytes was similar to that of the uninjected oocytes regardless

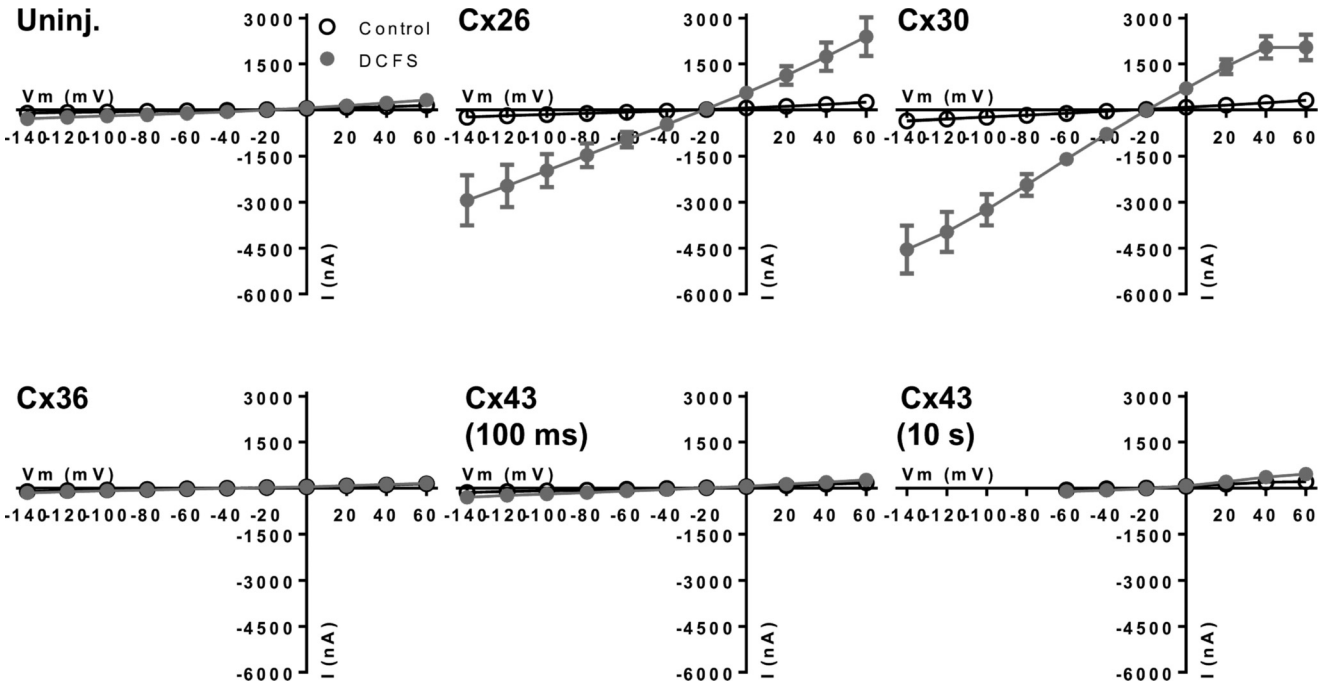

FIGURE 2. **Membrane currents of connexin-expressing oocytes following DCFS exposure.** *I/V* curves were measured from uninjected (*Uninj.*) and connexin-expressing oocytes in control solution containing 1 mM Ca^{2+} and 1 mM Mg^{2+} and after a 1-min exposure to DCFS. Currents were recorded from a holding potential of −50 mV by application of 100-ms voltage steps from −140 to +60 mV or 10-s voltage steps from −60 to +60 mV (Cx43 10 s) in intervals of 20 mV. The *I/V* relations were determined at the end of each voltage pulse and obtained from an average of 7–19 oocytes. Statistical significance (see text) was determined using two-way ANOVA with Holm-Šídák post hoc test comparing currents of uninjected and connexin-expressing oocytes in DCFS and Student's *t* test comparing uninjected and Cx43-expressing oocytes in DCFS following 10-s voltage steps. *Error bars* indicate S.E.

of the dye used (*i.e.* ethidium, Yo-Pro, or carboxyfluorescein; Fig. 4, *b–d*, *white bars*). Addition of BzATP (10 μM) did not affect dye uptake in the uninjected oocytes (Fig. 4, *b–d*, *black bars*) but promoted dye uptake in $P2X_7$-expressing oocytes as follows: ethidium (184 ± 29 *versus* 56 ± 8 a.u., $n = 7$, $p < 0.01$, *b*), Yo-Pro (4598 ± 1273 *versus* 1250 ± 167 a.u., $n = 6$, $p < 0.01$, *c*), and carboxyfluorescein (3479 ± 1155 *versus* 497 ± 114 a.u., $n = 6$, $p < 0.05$, *d*). Ethidium uptake in $P2X_7$-expressing oocytes was unaffected by removal of divalent cations from control solution (Fig. 4*b*, *gray bar*), whereas the combination of BzATP and DCFS resulted in a larger $P2X_7$-mediated ethidium uptake than seen with BzATP alone (compare Fig. 4, *b* and *e*). $P2X_7$ therefore mediated dye permeation and biphasic current in the absence of Px1, its proposed interaction partner for large pore formation.

Px1 and P2X$_7$ Co-expression—To test for a potential functional interaction between $P2X_7$ and Px1, these constructs were co-expressed in oocytes. In control solution, membrane conductance of Px1/$P2X_7$-expressing oocytes was comparable with that of Px1-expressing oocytes in size and rectification (compare Fig. 3*a* with Fig. 5*a*). Upon addition of BzATP to the test solution, the conductance increased and resembled that of non-rectifying $P2X_7$-expressing oocytes (compare Figs. 4*a* and 5*a*).

In control solution, the Px1/$P2X_7$-expressing oocytes were permeable to ethidium (369 ± 80 *versus* 60 ± 12 a.u., $n = 5–6$, $p < 0.01$, Fig. 3*b*) and Yo-Pro (5348 ± 984 *versus* 1214 ± 238 a.u., $n = 5$, $p < 0.01$, Fig. 3*c*) but not significantly to carboxyfluorescein (1137 ± 382 *versus* 503 ± 134 a.u., $n = 5–6$, Fig. 3*d*). These levels of dye uptake were similar to the observations with oocytes expressing only Px1 (Fig. 3, *b–d*). Exposure to DCFS did not increase ethidium uptake in Px1/$P2X_7$-expressing oocytes (Fig. 5*b*), and exposure to the $P2X_7$ agonist BzATP did not further increase the uptake of ethidium, Yo-Pro, or carboxyfluorescein (Fig. 5, *b–d*). Therefore, co-expression of Px1 and $P2X_7$ did not confer novel membrane conductance or dye uptake.

Potency of Brilliant Blue, Gadolinium, and Carbenoxolone—Several inhibitors are commonly used to identify different large pore channels in complex cell systems, although their potency and selectivity for the different (hemi)channels have not been fully characterized, limiting their utility (15, 16). We determined the potency of three commonly used inhibitors, Brilliant Blue, gadolinium (Gd^{3+}), and carbenoxolone in blocking ethidium uptake via connexin hemichannels, Px1, and $P2X_7$ expressed in oocytes. Cx26-expressing oocytes were not tested because they lack measurable ethidium permeability (Fig. 1*a*). The contribution from the native oocyte membrane (the uninjected oocytes) was subtracted to generate the inhibition curves. Brilliant Blue had the greatest potency against $P2X_7$ with an IC_{50} of 13.6 ± 2.3 μM, $n = 4$ (Fig. 6*a*) although an effect on Px1 and the Cx hemichannels was apparent at higher concentrations (IC_{50}: 82 ± 23, 169 ± 22, and 37 ± 6 μM for Cx30, Cx43, and Px1, respectively, $n = 3–4$). Gd^{3+} inhibited Cx30-, Cx36-, and $P2X_7$-mediated ethidium uptake with similar potency (IC_{50}: 2.4 ± 0.4, 2.0 ± 0.4, and 2.8 ± 1.0 μM for Cx30, Cx36, and $P2X_7$, respectively, $n = 3–6$, Fig. 6*b*), which is comparable with the IC_{50} value previously described for Cx43 (0.4 ± 0.1 μM (30)). Notably, the Gd^{3+} sensitivity of Cx30-mediated currents was higher than that obtained for dye uptake (0.3 ± 0.1 *versus* 2.4 ± 0.4 μM, $n = 6$, $p < 0.01$). In contrast,

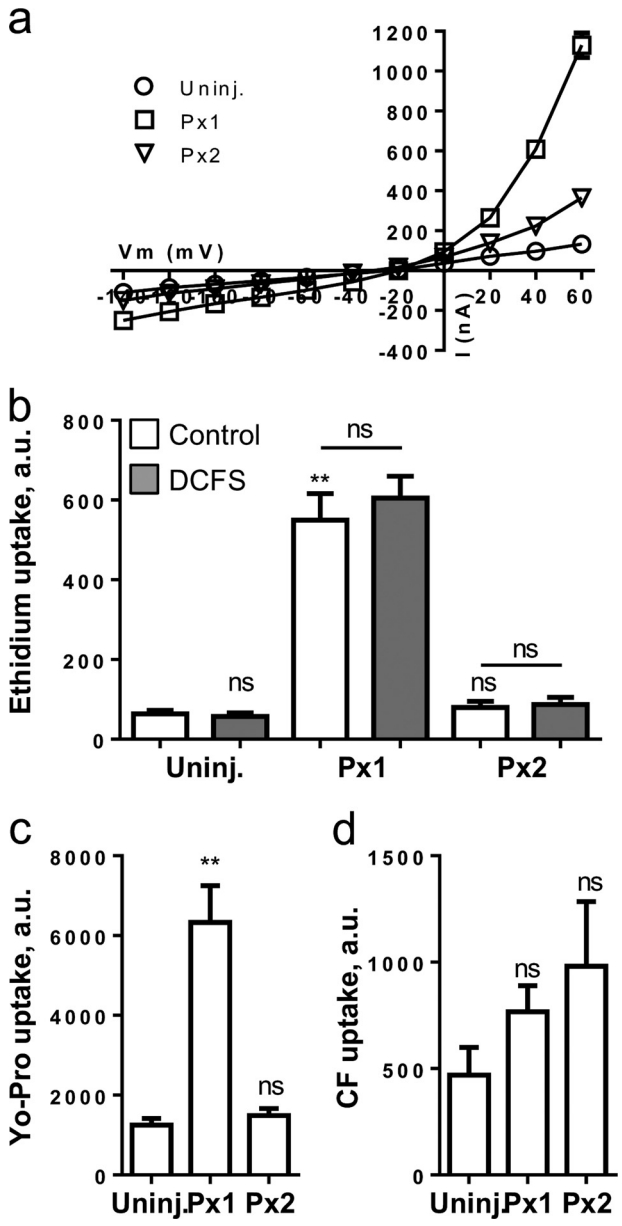

FIGURE 3. **Membrane currents and dye permeability of oocytes expressing Px1 and Px2.** *a,* summarized *I/V* relationships obtained with uninjected (*Uninj.*), Px1-, and Px2-expressing oocytes in control solution ($n = 9–17$ oocytes). *I/V* protocols were performed from a holding potential of −50 mV by application of 100-ms voltage steps from −140 to +60 mV in intervals of 20 mV and currents determined at the end of each pulse. Statistical significance was determined using two-way ANOVA with Holm-Šídák post hoc test. *b–d,* ethidium-, Yo-Pro-, and carboxyfluorescein uptake in control solution (*white bars*) or in DCFS (*gray bars*) for uninjected, Px1-, and Px2-expressing oocytes. $n = 4–9$ experiments; statistical significance was determined using Kruskal-Wallis with Dunn's post hoc test for *b* and *c* and one-way ANOVA with Holm-Šídák post hoc test for *d*. Statistical significance compared with uninjected oocytes is indicated directly *over the bar* and with *asterisks over the lines* for given in-group comparisons. *Error bars* indicate S.E. **, $p < 0.01$. *ns,* not significant.

Px1-mediated uptake was unperturbed by the addition of Gd^{3+} (Fig. 6*b*). At 1 mM carbenoxolone, the dye uptake tended to increase compared with that obtained at 200 μM, and the latter concentration was chosen as maximum to not obscure the fit. Px1, $P2X_7$, and Cx43 did not reach their IC_{50} values at this concentration (Fig. 6*c*); however, Cx30-mediated ethidium uptake was reduced to 46 ± 11% of control at 100 μM, $n = 4$. Curiously, Cx36 displayed carbenoxolone-induced increase in dye uptake, to 348 ± 45% of control at 200 μM, $n = 5$ (Fig. 6*d*). These inhibitor profiles demonstrate isoform-specific differences among the expressed (hemi)channels.

Hemichannel Activity in Cultured Rat Astrocytes—Having established key characteristics of possible astrocytic large pore channels in an isolated setting, we attempted to identify the molecular identity of the channel underlying DCFS-induced permeability in a native setting. First, we determined the DCFS-activated membrane current and dye permeability in primary cultures of rat cortical astrocytes. In conventional whole cell patch clamping, the intracellular content may be partially replaced with that of the pipette solution which may interfere with intracellular regulation of connexin hemichannels. The electrophysiological recordings were thus carried out using the perforated patch clamp technique to avoid replacing the cytosol with the pipette solution. The astrocytic membrane current was determined in control solution containing Ca^{2+} and Mg^{2+} and subsequently in DCFS (Fig. 7*a*, *top panel,* and summarized in *b*). The membrane current was not significantly increased in the absence of divalent cations (27 ± 7 *versus* 23 ± 8 pA/pF at +60 mV, $n = 11$ cells, $p > 0.9$) and was not significantly decreased upon addition of 50 μM Gd^{3+} to the DCFS (24 ± 8 pA/pF at +60 mV, $n = 10$, $p > 0.9$) (Fig. 7, *a* and *b*). In cultured rat astrocytes, no DCFS-induced, Gd^{3+}-sensitive membrane current above background was detected at the tested membrane potentials.

Dye permeability to ethidium and Yo-Pro was determined by adding dye to an astrocytic culture following determination of baseline background fluorescence. The dye uptake was subsequently monitored continuously. Cultured astrocytes were exposed to control solution (containing Ca^{2+} and Mg^{2+}) for 10 min followed by exposure to DCFS (see Fig. 7*c* for representative traces). The rate of dye uptake was quantified for the last 5 min in control solution and in DCFS, and the data were summarized and plotted as the "fold increase" in dye uptake rate upon removal of divalent cations. DCFS induced a significant increase in uptake of both fluorescent dyes (3.1 ± 0.3-fold for Yo-Pro uptake, $n = 5$, $p < 0.01$, and 1.4 ± 0.1-fold for ethidium uptake, $n = 9$, $p < 0.05$) (Fig. 7*d*, *gray bars*). The DCFS-induced uptake of Yo-Pro and ethidium were, however, insensitive to addition of 50 μM Gd^{3+} to the DCFS, $n = 5–9$ (Fig. 7*d*, *hatched bars* and *inset*). Thus, removal of divalent cations from the extracellular solution did promote dye uptake into cultured astrocytes, but the lack of Gd^{3+} sensitivity raised questions about the molecular mechanism underlying the dye uptake.

Dye Permeability of Cultured Astrocytes from WT and Cx43 cKO Mice—To resolve a putative role of Cx43 in astrocytic dye uptake, DCFS-induced ethidium and Yo-Pro uptake were determined, in parallel, in cultured astrocytes from wild-type (*WT*) and Cx43 cKO mice. Ethidium and Yo-Pro were added simultaneously, and the dye uptake was monitored as described above. Similar to the observations in rat astrocytes, a basal dye uptake was observed in control solution containing Ca^{2+} and Mg^{2+} (Fig. 8*a*). Following exposure to DCFS, the dye uptake of WT astrocytes increased to 1.12 ± 0.04-fold of the control for ethidium and 1.39 ± 0.09-fold for Yo-Pro ($n = 35$ experiments,

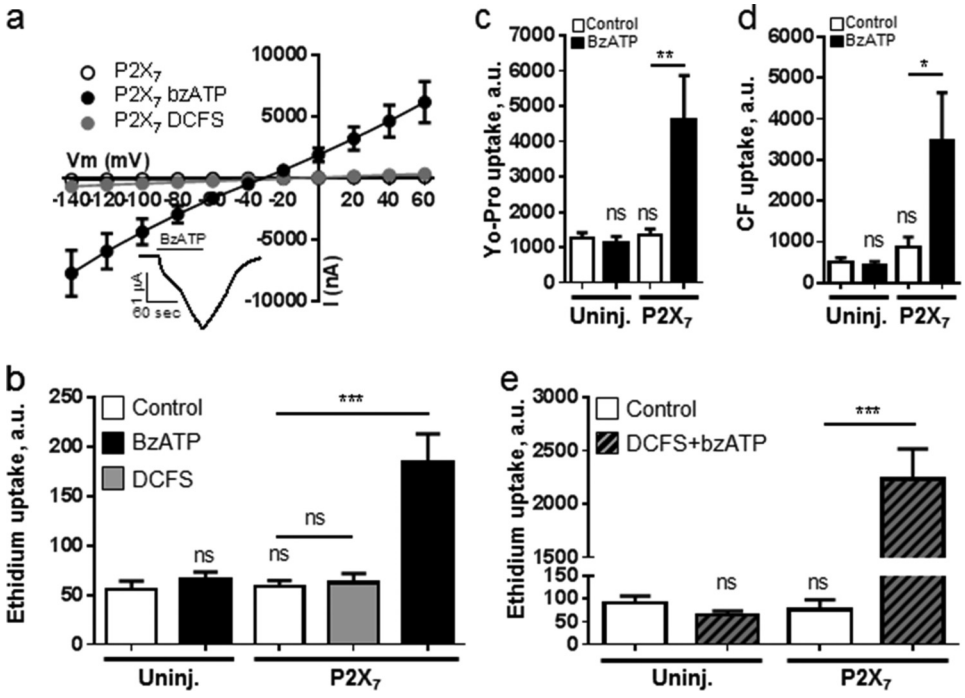

FIGURE 4. **$P2X_7$ expression gives large membrane currents and dye permeability following exposure to BzATP.** *a,* summarized *I/V* curves from $P2X_7$-expressing oocytes in control solution, following 1 min in BzATP (30 μM) or in DCFS ($n = 10–12$ oocytes). Statistical significance was determined using two-way ANOVA with Holm-Šídák post hoc test. *Inset,* representative trace of BzATP-induced membrane conductance in $P2X_7$-expressing oocyte measured at −50 mV. *b–d,* ethidium-, Yo-Pro-, and carboxyfluorescein uptake in uninjected (*Uninj.*) and $P2X_7$-expressing oocytes in control solution (*white bars*), control solution with BzATP (10 μM, *black bars*), or in DCFS (*gray bar*), $n = 6–7$ experiments. *e,* ethidium uptake in uninjected and $P2X_7$-expressing oocytes in control solution (*white bars*) or DCFS solution with BzATP (10 μM, *gray hatched bars*), $n = 3$ experiments. Statistical significance was determined using one-way ANOVA with Holm-Šídák post hoc test and indicated directly over bars for difference compared with uninjected oocytes and over lines for the given in-group comparisons. *Error bars* indicate S.E. *, $p < 0.05$; **, $p < 0.01$; ***, $p < 0.001$. *ns,* not significant.

$p < 0.05$) (Fig. 8*b*). However, we detected no significant difference between the DCFS-induced uptake in WT and Cx43 cKO astrocytes with ethidium (1.12 ± 0.04, $n = 35$ for WT *versus* 0.95 ± 0.06, $n = 18$ for Cx43 cKO, $p > 0.35$) and Yo-Pro (1.39 ± 0.09, $n = 35$ for WT *versus* 1.29 ± 0.16, $n = 18$ for Cx43 cKO, $p > 0.45$) (Fig. 8*b*). It is important to note that cells exposed to control solution for time periods similar to those in which we tested DCFS revealed no difference in dye uptake as a function of time ($n = 5$, $p > 0.75$, data not shown). In conclusion, DCFS-induced uptake of ethidium and Yo-Pro in mouse astrocytes was minor and independent of Cx43 expression.

Cx43 in Rat C6 Glioma Cells—With the genetic approach above providing evidence against a significant contribution from Cx43 in DCFS-induced dye uptake in cultured astrocytes, we next tested the C6 glioma cell line, with negligible endogenous expression of connexins and pannexins (50, 51), against C6 cells heterologously expressing Cx43. The cDNA encoding Cx43 was transduced into the genome of the native C6 cells. Cx43 was not detectable in WT C6 cells but was clearly seen in cells transduced with Cx43 (Fig. 9*a*). Wild-type C6 cells and Cx43-expressing C6 cells were exposed to ethidium in a sequence of solutions as follows: control solution followed by DCFS and subsequently by DCFS plus EDTA (to ensure complete chelation of any residual divalent cations and therefore increase the possibility for detection of Cx43-mediated dye uptake). Cellular fluorescence was monitored continuously (Fig. 9*b*). The native and transduced cells displayed comparable rates of ethidium uptake (Fig. 9*b*), as summarized in Fig. 9*c* ($n = 3$ matched experiments with a total of 52 and 49 cells for WT and Cx43, respectively). The rates of ethidium uptake during these experiments never varied from those seen in C6 Cx43 cells continuously exposed to control solution containing 1.8 mM Ca^{2+} for the same period of time ($n = 3$ experiments with 28 cells, data not shown). In summary, no increase in dye uptake of C6 cells was produced by DCFS regardless of whether Cx43 was expressed or not.

DISCUSSION

We have in this study demonstrated that large pore channels of different molecular identities have overlapping, although isoform-specific, channel characteristics when expressed heterologously in *Xenopus* oocytes. Curiously, we observed no direct link between atomic ion conductance and dye permeability for the different pores.

Removal of divalent cations from the extracellular solution induces hemichannel opening in a variety of connexins (6, 8, 11, 29), and accordingly, we observed hemichannel activity in oocytes expressing Cx26, Cx30, and Cx43 upon exposure to DCFS. Cx36, however, was constitutively permeable to ethidium and unaffected by the concentration of divalent cations in the extracellular solution. Cx43 displayed a slight ethidium uptake in the presence of 1 mM Ca^{2+}, which is in accordance with our previous findings where Cx43 is only partially closed at this Ca^{2+} concentration (30). The sensitivity to extracellular Ca^{2+} for dye uptake through Cx30 was distinct from that of Cx43, with a steeper slope and near-complete inhibition for Cx30-mediated dye uptake at 0.5 mM Ca^{2+}, although the Cx30 and Cx43 IC_{50} values for Ca^{2+} were similar (this study and see

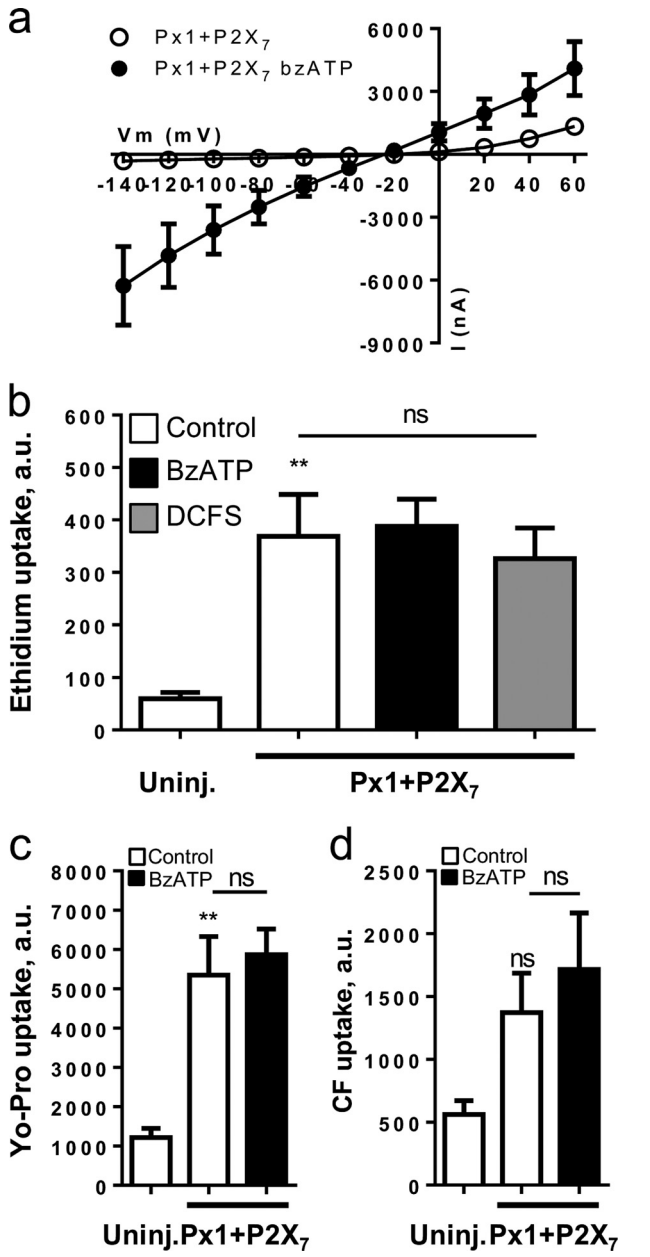

FIGURE 5. **No additive effect of co-expressing Px1 and $P2X_7$ on membrane conductance and dye permeability.** *a,* summarized *I/V* curves from Px1/$P2X_7$-expressing oocytes in control solution (*white symbols*) or 30 μM BzATP (*black symbols*), $n = 7–8$. *b–d,* ethidium-, Yo-Pro-, and carboxyfluorescein uptake in uninjected (*Uninj.*) and Px1/$P2X_7$-expressing oocytes in control solution (*white bars*), control solution with 10 μM BzATP (*black bars*), or DCFS (*gray bar*), $n = 5$ experiments. Statistical significance was determined using one-way ANOVA with Holm-Šídák post hoc test and indicated directly over bars for difference compared with uninjected oocytes and over lines for the given in-group comparisons. *Error bars* indicate S.E. **, $p < 0.01$. *ns,* not significant.

Ref. 30). It must be noted, however, that removal of divalent cations may have a variety of secondary cellular effects such as (i) membrane depolarization which may (52) or may not (30, 53) promote Cx43 hemichannel opening, and (ii) changes in intracellular Ca^{2+} concentration that may, in itself, affect hemichannel opening (54, 55). Once the opening was induced in the respective hemichannels, the permeation pattern differed among the connexins: Cx30-expressing oocytes displayed Gd^{3+}-sensitive ion conductance and permeability to both ethidium, Yo-Pro, and propidium, whereas Cx36- and Cx43-expressing oocytes displayed only ethidium permeability (in a Gd^{3+}-sensitive fashion), and Cx26-expressing oocytes solely exhibited Gd^{3+}-sensitive membrane conductance and no dye permeability. However, it should be noted that oocytes expressing Cx36 and Cx43 had a tendency to reduced Yo-Pro and propidium uptake, although not to a statistically significant degree. This could indicate that another minor Yo-Pro/propidium-permeable transport system, native to the oocyte membrane, may be outcompeted by the experimental overexpression of connexins. Additionally, the Yo-Pro/propidium uptake and the gadolinium-sensitive component appeared greater for Cx26-expressing than for Cx36- and Cx43-expressing oocytes. Thus, we cannot exclude slight Cx26-mediated dye permeability in the present setting. These data may align with previously published data on limited DCFS-induced Cx26-mediated dye uptake in Cx-expressing HeLa cells: the low number (21%) of cells permitting DCFS-induced dye uptake (56) and the limited (~2-fold) DCFS-induced increase in dye uptake (57).

Activation of hemichannel-mediated atomic ion conductance by removal of extracellular divalent cations has previously been demonstrated at physiologically relevant membrane potentials for Cx26 and Cx30 expressed in *Xenopus* oocytes or mammalian cell lines (6, 8, 30), whereas it is often reported that highly positive membrane potentials (>40 mV) or addition of cytokines is required to observe Cx43-mediated conductance in mammalian cell systems (4, 25, 26, 58). Lack of Cx36 hemichannel-mediated conductance has previously been demonstrated (59, 60). Interestingly, although Cx36, in its gap-junction configuration, has an extremely low single channel conductance (10–15 pS), Cx36 gap junctions are nevertheless permeable to the fluorescent dyes Lucifer Yellow and ethidium (61, 62).

Our data indicate that the connexin hemichannels have distinct extracellular Ca^{2+}-mediated activation regimes and display distinct permeability toward ions as well as toward dyes of different molecular composition. Although the difference may seem more subtle, cell to cell gap junctional channels do share peculiar relations between their single channel conductance and selectivity. A thorough comparison by Harris and Locke (63) showed no correlation between single channel conductance and the selectivity for atomic cations *versus* anions. When dealing with molecules, the complexity only increases, and some connexins, such as Cx30, are in their gap junction constellation reported to discriminate molecules mainly based on charge (64), whereas the Cx43 permeability profile depends more on size (65).

A disconnect between hemichannel-mediated dye permeability and conductance, such as that observed in this study for Cx26, Cx36, and Cx43, seems counterintuitive due to the ~15 Å large pore reported in the crystal structures of connexins 26 and 43 (66, 67). However, inclusion of amino acid side chains lining the pore will reduce the pore size to ~5 Å (66). In addition, the C and N termini may create an intracellular plug with potential participation in channel gating (68). Connexin hemichannels in their intact and functional form may therefore not operate with an open ~15 Å large pore but may, via the amino

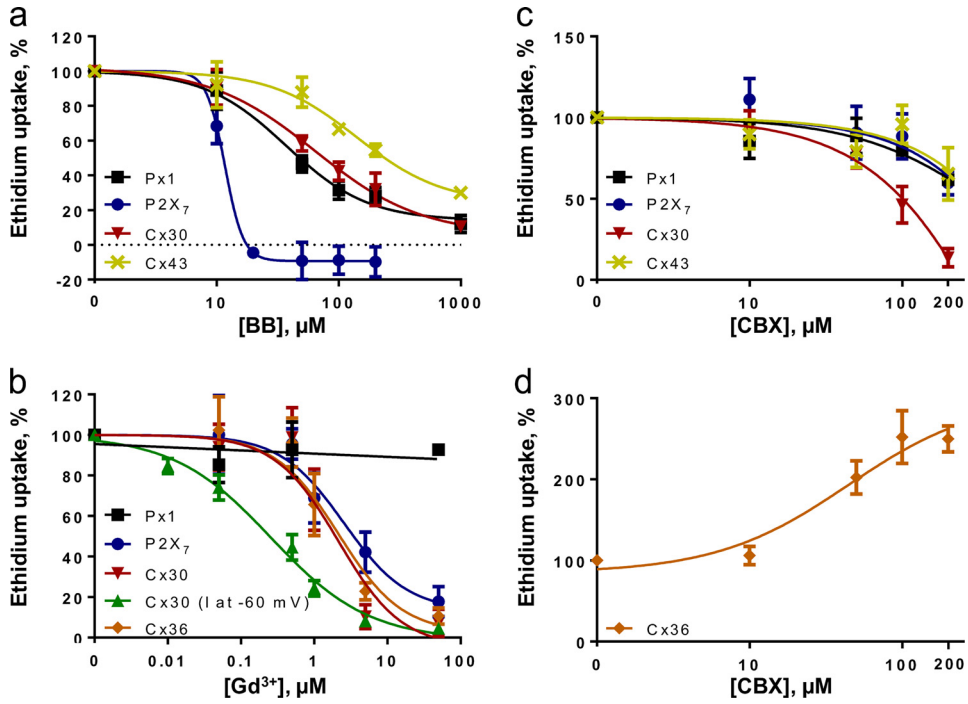

FIGURE 6. **Dye uptake in the presence of Brilliant Blue, gadolinium, and carbenoxolone.** Ethidium uptake or membrane conductance (Cx30, gadolinium; *I* at −60 mV) was determined in Cx30-, Cx36-, Cx43-, Px1-, and $P2X_7$-expressing oocytes exposed to either Brilliant Blue (*BB*), gadolinium (Gd^{3+}), or carbenoxolone (*CBX*). Connexin-mediated uptake was determined in DCFS; Px1-mediated uptake was obtained in control solution, and BzATP (10 μM) was employed to obtain the $P2X_7$-mediated uptake. Following subtraction of the contribution from the uninjected oocytes, ethidium uptake as a function of inhibitor concentration was fitted using linear regression (Gd^{3+}, Px1) or a three (Brilliant Blue and carbenoxolone; Cx30, Gd^{3+}; Cx30, Cx36, and $P2X_7$) or four (Brilliant Blue; Cx43, Px1, and $P2X_7$) parameter logistic equation. *a,* uptake with Brilliant Blue concentrations from 0 to 1000 μM, $n = 3–4$ experiments with 5–6 points. *b,* uptake with Gd^{3+} from 0 to 1000 μM, $n = 3–6$ experiments with 6–7 points (2–4 for Px1). Included is the Cx30-mediated current, obtained by a two-electrode voltage clamp as in Fig. 2 and fitted using a four-parameter logistic equation. *c* and *d,* uptake with carbenoxolone from 0 to 200 μM, $n = 3–5$ experiments with 5 points. Each data point averages *n* experiments; *line* indicates best fit, and IC_{50} was determined as the average of independent regression analyses.

acid side chains lining the pore, their termini, and extracellular loops, generate a form of isoform-specific pore selectivity filters as well as permeant-specific gating properties. It must be noted that molecular mechanisms allowing permeability of large molecules, while concomitantly excluding ions, are observed in an unrelated class of large pore membrane channels, the aquaglyceroporins such as AQP9 (69, 70).

Pannexins belong to another class of large pore channels that appear not to form intercellular junctional pores (71). Px1 has been suggested as an alternative to the proposed Cx43-mediated astrocytic hemichannel activity (9, 72) as it shares key properties with the connexin hemichannels, including dye permeability, ATP release, and propagation of Ca^{2+} waves (14, 15, 71). Oocytes expressing either Px1 or Px2 displayed an outwardly rectifying conductance at positive membrane potentials, which is characteristic for pannexins whether heterologously expressed in mammalian cells or *Xenopus* oocytes (9, 44, 71, 73). The Px2-expressing oocytes displayed smaller membrane conductance than that of the Px1-expressing oocytes, but without the knowledge of unit expression level, we cannot, at present, exclude that the difference in membrane conductance originates from lower expression levels of Px2. No dye uptake was detectable in the Px2-expressing oocytes, although Px1-expressing oocytes displayed a constitutively large uptake of ethidium and Yo-Pro. Notably, the large dye uptake was readily observed at basal negative membrane potentials, whereas the membrane conductance appeared exclusively at positive membrane potentials in a strictly voltage-gated manner. In analogy with the connexin hemichannels, pannexins therefore possess the ability to distinguish between fluorescent dyes and atomic ions with a distinct gating paradigm for each permeant. The Px1-mediated ethidium uptake was not affected by removal of divalent cations, and with this lack of DCFS-induced opening, it appears that Px1 and Cx43 may well open under distinct physiological conditions, and therefore each serve a different physiological purpose in native cells.

P2X purinergic receptors are agonist-induced ion channels, some of which (*e.g.* $P2X_7$) undergo pore dilation upon prolonged activation, allowing for permeation of large molecules and/or increased current (40, 41, 74). Px1 has been proposed to enter into a functional complex with $P2X_7$ and act as the molecular origin of the large pore (42–44). BzATP-induced nonrectifying membrane conductance was observed in $P2X_7$-expressing oocytes with the previously reported characteristics of $P2X_7$-mediated conductance (10, 75). Expression of $P2X_7$ allowed for agonist-induced permeation of three different fluorescent dyes (ethidium, Yo-Pro, and carboxyfluorescein). Although a few reports suggest inherent lack of dye permeability in $P2X_7$ (42–44), $P2X_7$-mediated large molecule and fluorescent dye permeability (in the absence of Px1) have, in analogy with the present data, been documented in mammalian cell lines (40, 76), thus arguing against the proposed requirement for Px1 to act as the large pore channel during $P2X_7$-mediated dye uptake.

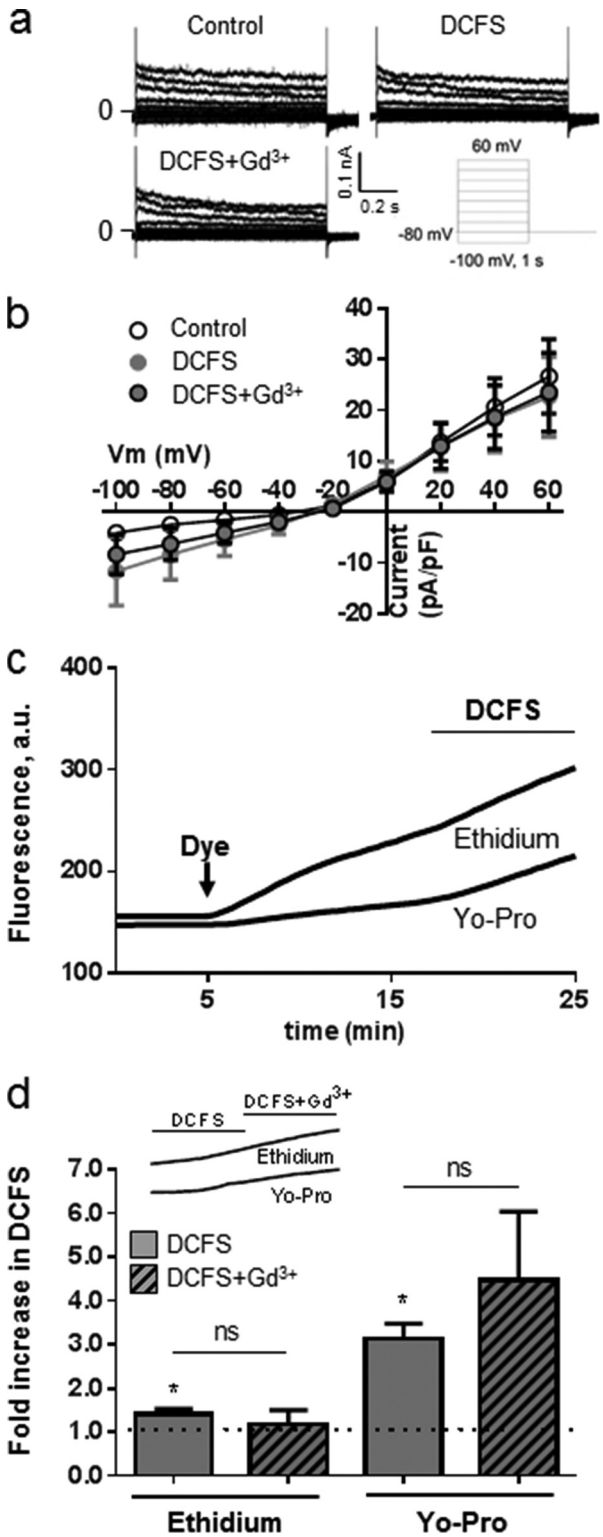

FIGURE 7. **Dye permeability but not membrane conductance of rat cortical astrocytes is increased following exposure to DCFS.** *a,* membrane conductance obtained with the perforated patch clamp technique was recorded from a holding potential of −80 mV by application of 1-s voltage steps from −100 to +60 mV in intervals of 20 mV in control solution with 1.8 mM Ca^{2+} and 1 mM Mg^{2+} present followed by DCFS and finally by DCFS + 50 μM Gd^{3+}. *b,* summarized *I/V* relations as performed in *a* and determined at the end of pulses, with currents in control solution (*white symbols*), DCFS (*gray symbols*), and DCFS + 50 μM Gd^{3+} (*black-bordered gray symbols*). $n = 10–11$, currents were normalized to membrane capacitance (pA/pF). *c,* dye uptake visualized by fluorescence microscopy with representative traces of ethidium and Yo-Pro uptake in cells in control solution followed by exposure to DCFS. *d,* summarized Yo-Pro and ethidium uptake rates in DCFS in the absence (*gray bars*) or presence (*hatched bars*) of 50 μM Gd^{3+} from experiments as in *c* (see *inset*) with uptake rates normalized to uptake in control solution, $n = 5$ and 9 experiments for Yo-Pro and ethidium, respectively. Statistical significance was determined using one-way (*c* and *d*) or two-way (*b*) ANOVA with Holm-Šídák post hoc test, and one sample *t* test against the value 1.0 for DCFS (*d*). Statistical significance is indicated over bars for difference compared with uptake in control solution and over lines for the given in-group comparisons. *Error bars* indicate S.E. *, $p < 0.05$; **, $p < 0.01$; *ns,* not significant.

The *I/V* relationship of the membrane conductance observed in Px1/$P2X_7$-expressing oocytes was in control solution indistinguishable from that of the Px1-expressing oocytes and in the presence of BzATP indistinguishable from that of the $P2X_7$-expressing oocytes, thus indicating that both large pore channels are functionally expressed and capable of conducting ions, independently of each other, in a nonsynergistic way upon co-expression in *Xenopus* oocytes. The BzATP-induced current traces obtained in $P2X_7$-expressing oocytes consistently presented with a shoulder prior to full channel opening. This particular pattern has previously been observed in mammalian cells and was suggested to originate from initial BzATP-induced activation of $P2X_7$ (the shoulder) and a subsequent $P2X_7$-mediated activation of Px1 (the full current activation) (42). Observation of such a shoulder in oocytes exclusively expressing $P2X_7$ suggests that this current pattern is inherent to $P2X_7$ and thus argues against the requirement of Px1 for full activation. Co-expression of Px1 and $P2X_7$ did not lead to synergistic effects on the dye uptake. In the absence of $P2X_7$ agonist, Px1/$P2X_7$-expressing oocytes displayed the large constitutive dye uptake also observed in oocytes expressing Px1 alone. Curiously, for reasons presently unknown, BzATP failed to induce further dye uptake in Px1/$P2X_7$-expressing oocytes. One possible explanation for this discrepancy could be the previously reported BzATP-mediated inhibition of Px1 (77) that we, however, did not observe in this study. Taken together, it appears that $P2X_7$ possesses the ability to undergo pore dilation and thus, in the absence of Px1, allow for permeation of fluorescent dyes. Although $P2X_7$ receptors have the capability to function independently of Px1, our data by no means preclude that Px1 may be activated by other receptors, as has been demonstrated for α-adrenergic and NMDA receptors (78, 79).

A range of studies has been carried out on complex cell systems and molecular identity to a certain transport pathway assigned partly by the aid of pharmacological inhibitors (42, 43, 60, 80, 81). Although several of these agents act in a potent fashion, their specificity is either nonexisting or awaits determination, which complicates finite interpretation of the individual role of the different large pore channels (15, 16, 82). A recent approach that may offer more specificity has been the mimetic peptide Gap19, which inhibited Cx43 hemichannels without affecting Cx40 or Px1 (83). In this study, Brilliant Blue was a potent inhibitor of $P2X_7$-mediated dye uptake in accordance with Ref. 84, but it also affected connexin hemichannels and Px1 albeit at slightly higher concentrations (the latter previously observed by (77)). Gadolinium, however, inhibited dye uptake of all tested connexin hemichannels and $P2X_7$ to a

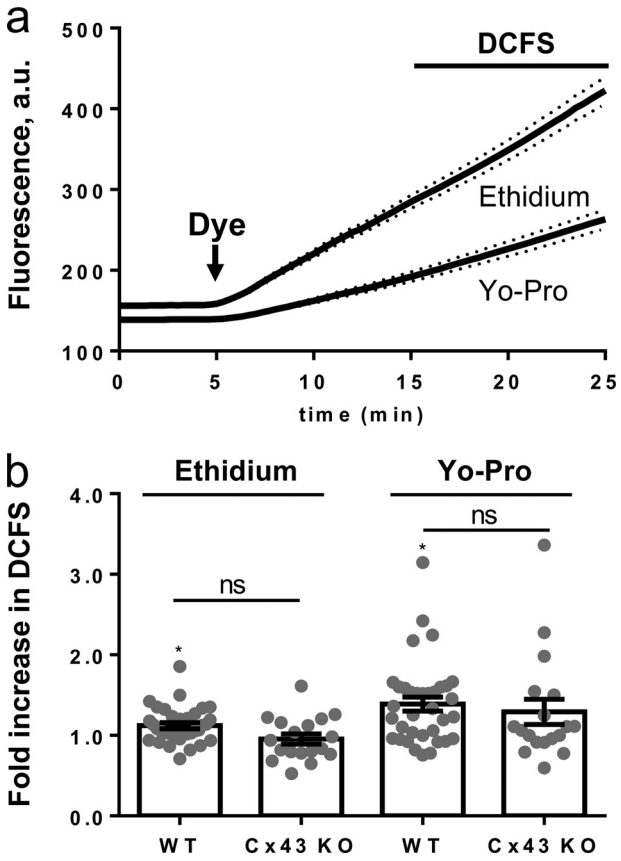

FIGURE 8. **Dye permeability of wild-type (WT) and Cx43$^{-/-}$ (Cx43 KO) mouse cortical astrocytes is comparable following exposure to DCFS.** *a,* traces of WT mouse astrocyte ethidium and Yo-Pro uptake in the presence of 1.8 mM extracellular Ca^{2+} and 1 mM Mg^{2+} followed by exposure to DCFS as in Fig. 7, $n = 32$, *dashed lines* indicate S.E. *b,* summarized Yo-Pro and ethidium uptake rates in DCFS with data obtained as in *a* with uptake rates given relative to uptake in control solution, $n = 35$, and 18 experiments for WT and Cx43 KO, respectively. Statistical significance was determined using one sample *t* test against the value 1.0, and between WT and KO using Kruskal-Wallis with Dunn's post hoc test. Statistical significance is indicated on top of bars for difference compared with uptake in control solution and on lines for the given in-group comparisons. *Error bars* indicate S.E. *, $p < 0.05$; *ns,* not significant.

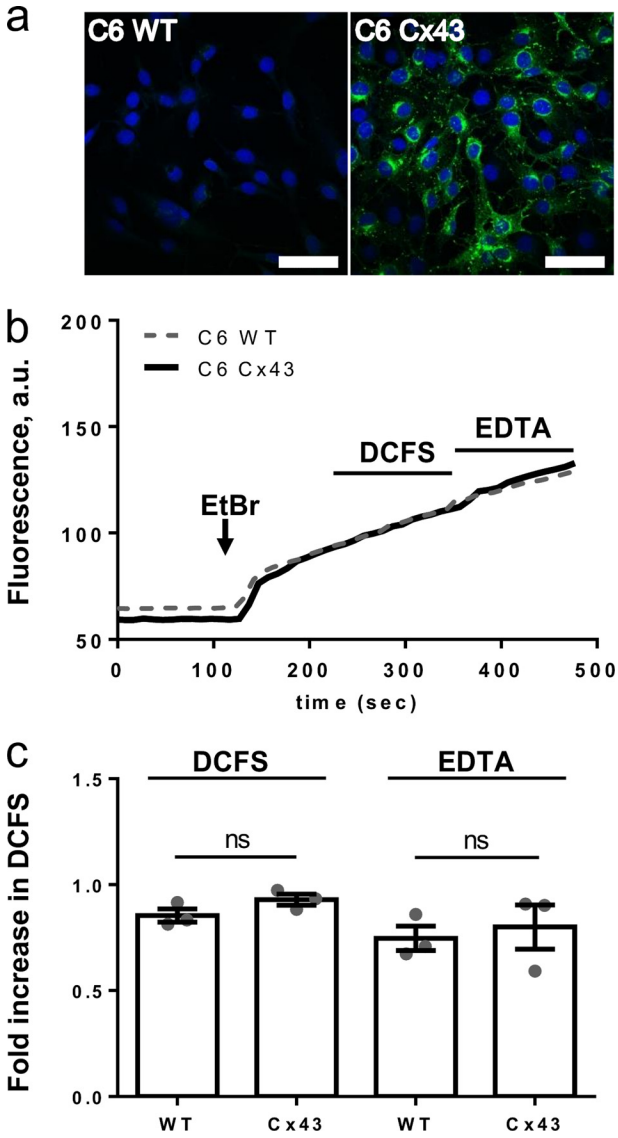

FIGURE 9. **Removal of divalent cations does not stimulate ethidium uptake in Cx43-expressing C6 cells.** *a,* native (*C6 WT*) and Cx43-expressing C6 rat glioma cells (*C6 Cx43*) were stained with an anti-Cx43 antibody (*green*), and the nucleus was visualized with DAPI (*blue*); *bar,* 50 μm. *b,* ethidium uptake by C6 glioma cells seeded on coverslips was visualized by fluorescence microscopy. Representative traces of ethidium fluorescence in C6 Cx43 shown as a *thick black trace* and C6 WT as a *gray dashed trace* in the presence of 1.8 mM extracellular Ca^{2+} and 1 mM Mg^{2+} followed by exposure to DCFS and finally in EDTA-containing DCFS (*EDTA*). *c,* summarized ethidium uptake in DCFS and EDTA, with data obtained as in *b*, and values given relative to the uptake in control solution, $n = 3$ matched experiments; statistical significance was determined using one-way ANOVA with Holm-Šídák post hoc test and indicated on lines for the given in-group comparisons. *ns,* not significant.

similar extent while displaying a higher potency toward Cx30-mediated current *versus* dye uptake. Px1 was completely insensitive to gadolinium even at very high concentrations, as previously observed (44, 85). Carbenoxolone, curiously, increased Cx36-mediated dye uptake, inhibited Cx30-mediated dye uptake, and displayed a relatively low potency toward Cx43, Px1, and $P2X_7$. The increase in Cx36-mediated uptake may reflect relief from inhibition by intramembrane arachidonic acid as reported for short chain alcohols on Cx36 but not Cx43 gap junctional channels (86). Carbenoxolone has previously been reported to display a partial effect on Yo-Pro uptake in Px1-expressing HEK293 cells (87), whereas much higher potency is found in electrophysiological experiments in both oocytes and complex cell systems expressing Px1 (73, 85). Based on the higher Gd^{3+} sensitivity observed with Cx30-mediated current *versus* dye uptake (this study), it is possible that Px1-mediated currents and dye uptake are differentially affected by carbenoxolone. Isoform-specific inhibitor profiles thus exist among the connexins in their hemichannel configuration, and the inhibitor potency varies with transport mode (dye *versus* current). These data now add, to the already extensive list of promiscuous large pore channel inhibitors (15, 82), Gd^{3+} as a potent $P2X_7$-inhibitor, Brilliant Blue as a connexin hemichannel inhibitor, and carbenoxolone as more potent toward Cx30 than Cx43. However, according to the present data, gadolinium provides a useful tool with which to distinguish between pannexin- and connexin-hemichannel-mediated dye permeability (while bearing in mind the plethora of other Gd^{3+}-sensitive channels expressed in native cells).

Heterologous expression systems such as *Xenopus* oocytes and mammalian cell lines are designed to overexpress a given protein to an extent where the background permeabilities become negligible. The advantage thereof is to provide a setting in which the biophysical properties of a transport protein of interest can be determined. It must, however, be emphasized that in expression systems and cultured cells, one cannot be assured of correct protein processing and/or the presence of any required cofactor, etc. Observations obtained with gross overexpression of a given protein could, however, not be detectable in a native setting where expression may be much lower and a range of other transport proteins may contribute to the measured transport. We therefore aimed to determine the large pore channel activated by DCFS in astrocytes using the characteristics identified in this study. In cultured rat cortical astrocytes, however, we detected no evidence of a DCFS-induced Gd^{3+}-sensitive membrane current at physiologically relevant membrane potentials. In a previously published report, DCFS-induced conductance was detected in a subset of tested astrocytes (60%; 3 out of 5 cells): when observed, the conductance occurred at all tested membrane potentials (88), which differs from the Cx43-mediated conductance reportedly arising predominantly at highly positive membrane potentials in Cx43-expressing HeLa cells (4, 25). It is, at present, not clear why different current patterns are obtained in astrocytes exposed to DCFS, Cx43-expressing HeLa cells, and *Xenopus* oocytes, but differences in electrophysiological approaches may play a role (sharp electrode *versus* fast whole cell patch *versus* perforated whole cell patch). The astrocytic data of this study are in agreement with data from Cx43-expressing HeLa cells and *Xenopus* oocytes, thus showing a lack of significant Cx43-mediated DCFS-induced current at negative membrane potentials (4, 28, 30). In rat astrocytes, we detected a DCFS-induced increase in uptake of ethidium and Yo-Pro which was, however, insensitive to Gd^{3+} and therefore unlikely to be Cx43-mediated. A few research groups have previously reported DCFS-induced Lucifer Yellow uptake in astrocytic cultures (29, 89), whereas other groups failed to detect DCFS-induced permeability to ethidium or calcein when astrocytes were grown in conventional medium (53, 90). With the lack of a specific Cx43 inhibitor, we took advantage of the conditional Cx43 knock-out mice but detected no significant difference between the DCFS-induced uptake of ethidium or Yo-Pro in a comprehensive series of parallel experiments on astrocytes obtained from these animals in comparison with those obtained from WT mice. Cx43-expressing C6 cells (transduced into the genome rather than transfected and hence presumably not overexpressing Cx43 to the same level as that obtained by transient transfections) have previously been shown to support gap-junctional coupling (91). Nevertheless, these cells did not present with DCFS-induced dye uptake under the employed experimental conditions. Although Cx43 hemichannels are indeed able to transport small quantities of ethidium upon exposure to DCFS when overexpressed in a cellular system (this study and Refs. 4, 11), in a complex system with parallel dye/ion transport routes their contribution to dye/ion transport may simply not be detectable upon removal of divalent cations. However, a range of experimental factors may well promote experimentally detectable Cx43-mediated dye uptake and ion conductance, *e.g.* species-specific channel function, culture conditions, choice of fluorescent dye, presence of cytokines, the metabolic state of the cells, excessively positive membrane potentials, and/or the mechanism of solution exchange. In relation to the latter, removal of control solution by suction and subsequent addition of test solution may well induce a mechanical stimulus, which in itself has been shown to affect Cx43 hemichannel opening under calcium-free conditions (88).

In conclusion, we have demonstrated that a range of neuronal and astrocytic channels, when heterologously expressed, display type- and isoform-specific extracellular Ca^{2+} sensitivity and permeation. Although the central pore of these channels is of relatively large diameter, molecular mechanisms appear to be in place to prevent nonselective free diffusion of molecules upon channel opening. Several of the tested (hemi)channels possess the ability to gate conductance and fluorescent dye permeability independently. We detected no obvious DCFS-induced Cx43-dependent dye uptake in cultured astrocytes and conclude, under our experimental conditions, that although Cx43 may indeed be able to allow dye permeation and conductance under certain experimental conditions, their contribution to these transport parameters may, upon removal of divalent cations, be negligible in complex native cells such as astrocytes. It seems probable, however, that future studies may reveal additional variables that impact the function and gating of Cx43 hemichannels in astrocytes.

Acknowledgments—The assistance of Brian Roland Larsen, Ninna Buch Petersen, Charlotte Goos Iversen, Danielle Hanssen, and Catia Correa Goncalves Andersen is gratefully acknowledged. We are grateful to Thomas W. White, Stony Brook University, New York; Klaus Willecke, Bonn University, Germany; Gunter Schmalzing, University of Kaachen, Germany (via Rainer Schreiber, University of Regensburg, Germany); Robert Bruzzone (via Gina Sosinsky, University of California at San Diego School of Medicine); and Zealand Pharma, Denmark, for providing the cDNA encoding hCx26, mCx30, mCx36, rCx43, hP2X$_7$, rPx1, and rPx2.

REFERENCES

1. Bruzzone, R., Hormuzdi, S. G., Barbe, M. T., Herb, A., and Monyer, H. (2003) Pannexins, a family of gap junction proteins expressed in brain. *Proc. Natl. Acad. Sci. U.S.A.* **100,** 13644–13649
2. Cheung, K. K., Chan, W. Y., and Burnstock, G. (2005) Expression of P2X purinoceptors during rat brain development and their inhibitory role on motor axon outgrowth in neural tube explant cultures. *Neuroscience* **133,** 937–945
3. Nagy, J. I., Dudek, F. E., and Rash, J. E. (2004) Update on connexins and gap junctions in neurons and glia in the mammalian nervous system. *Brain Res. Brain Res. Rev.* **47,** 191–215
4. Contreras, J. E., Sáez, J. C., Bukauskas, F. F., and Bennett, M. V. (2003) Gating and regulation of connexin 43 (Cx43) hemichannels. *Proc. Natl. Acad. Sci. U.S.A.* **100,** 11388–11393
5. Kang, J., Kang, N., Lovatt, D., Torres, A., Zhao, Z., Lin, J., and Nedergaard, M. (2008) Connexin 43 hemichannels are permeable to ATP. *J. Neurosci.* **28,** 4702–4711
6. Sánchez, H. A., Mese, G., Srinivas, M., White, T. W., and Verselis, V. K. (2010) Differentially altered Ca^{2+} regulation and Ca^{2+} permeability in Cx26 hemichannels formed by the A40V and G45E mutations that cause keratitis ichthyosis deafness syndrome. *J. Gen. Physiol.* **136,** 47–62
7. Schock, S. C., Leblanc, D., Hakim, A. M., and Thompson, C. S. (2008) ATP

release by way of connexin 36 hemichannels mediates ischemic tolerance *in vitro*. *Biochem. Biophys. Res. Commun.* **368,** 138–144
8. Valiunas, V., and Weingart, R. (2000) Electrical properties of gap junction hemichannels identified in transfected HeLa cells. *Pflugers Arch.* **440,** 366–379
9. Iglesias, R., Dahl, G., Qiu, F., Spray, D. C., and Scemes, E. (2009) Pannexin 1: the molecular substrate of astrocyte "hemichannels". *J. Neurosci.* **29,** 7092–7097
10. Surprenant, A., Rassendren, F., Kawashima, E., North, R. A., and Buell, G. (1996) The cytolytic P2Z receptor for extracellular ATP identified as a P2X receptor (P2X7). *Science* **272,** 735–738
11. Orellana, J. A., Díaz, E., Schalper, K. A., Vargas, A. A., Bennett, M. V., and Sáez, J. C. (2011) Cation permeation through connexin 43 hemichannels is cooperative, competitive and saturable with parameters depending on the permeant species. *Biochem. Biophys. Res. Commun.* **409,** 603–609
12. Poornima, V., Madhupriya, M., Kootar, S., Sujatha, G., Kumar, A., and Bera, A. K. (2012) P2X7 receptor-pannexin 1 hemichannel association: effect of extracellular calcium on membrane permeabilization. *J. Mol. Neurosci.* **46,** 585–594
13. Liu, H. T., Tashmukhamedov, B. A., Inoue, H., Okada, Y., and Sabirov, R. Z. (2006) Roles of two types of anion channels in glutamate release from mouse astrocytes under ischemic or osmotic stress. *Glia* **54,** 343–357
14. Scemes, E., Spray, D. C., and Meda, P. (2009) Connexins, pannexins, innexins: novel roles of "hemi-channels". *Pflugers Arch.* **457,** 1207–1226
15. Spray, D. C., Ye, Z. C., and Ransom, B. R. (2006) Functional connexin "hemichannels": a critical appraisal. *Glia* **54,** 758–773
16. Ye, Z. C., Oberheim, N., Kettenmann, H., and Ransom, B. R. (2009) Pharmacological "cross-inhibition" of connexin hemichannels and swelling activated anion channels. *Glia* **57,** 258–269
17. Dahl, G. (2007) Gap junction-mimetic peptides do work, but in unexpected ways. *Cell Commun. Adhes.* **14,** 259–264
18. Bargiotas, P., Krenz, A., Hormuzdi, S. G., Ridder, D. A., Herb, A., Barakat, W., Penuela, S., von Engelhardt, J., Monyer, H., and Schwaninger, M. (2011) Pannexins in ischemia-induced neurodegeneration. *Proc. Natl. Acad. Sci. U.S.A.* **108,** 20772–20777
19. Salas, E., Carrasquero, L. M., Olivos-Oré, L. A., Bustillo, D., Artalejo, A. R., Miras-Portugal, M. T., and Delicado, E. G. (2013) Purinergic P2X7 receptors mediate cell death in mouse cerebellar astrocytes in culture. *J. Pharmacol. Exp. Ther.* **347,** 802–815
20. Suadicani, S. O., Brosnan, C. F., and Scemes, E. (2006) P2X7 receptors mediate ATP release and amplification of astrocytic intercellular Ca^{2+} signaling. *J. Neurosci.* **26,** 1378–1385
21. Chanson, M., Kotsias, B. A., Peracchia, C., and O'Grady, S. M. (2007) Interactions of connexins with other membrane channels and transporters. *Prog. Biophys. Mol. Biol.* **94,** 233–244
22. Iacobas, D. A., Iacobas, S., Urban-Maldonado, M., Scemes, E., and Spray, D. C. (2008) Similar transcriptomic alterations in Cx43 knockdown and knockout astrocytes. *Cell Commun. Adhes.* **15,** 195–206
23. Nicke, A., Kuan, Y. H., Masin, M., Rettinger, J., Marquez-Klaka, B., Bender, O., Górecki, D. C., Murrell-Lagnado, R. D., and Soto, F. (2009) A functional P2X7 splice variant with an alternative transmembrane domain 1 escapes gene inactivation in P2X7 knock-out mice. *J. Biol. Chem.* **284,** 25813–25822
24. Singh, D., and Lampe, P. D. (2003) Identification of connexin-43 interacting proteins. *Cell Commun. Adhes.* **10,** 215–220
25. Wang, N., De Bock, M., Antoons, G., Gadicherla, A. K., Bol, M., Decrock, E., Evans, W. H., Sipido, K. R., Bukauskas, F. F., and Leybaert, L. (2012) Connexin mimetic peptides inhibit Cx43 hemichannel opening triggered by voltage and intracellular Ca^{2+} elevation. *Basic Res. Cardiol.* **107,** 304
26. Wang, N., De Bock, M., Decrock, E., Bol, M., Gadicherla, A., Bultynck, G., and Leybaert, L. (2013) Connexin targeting peptides as inhibitors of voltage- and intracellular Ca^{2+}-triggered Cx43 hemichannel opening. *Neuropharmacology* **75,** 506–516
27. Cotrina, M. L., Lin, J. H., López-García, J. C., Naus, C. C., and Nedergaard, M. (2000) ATP-mediated glia signaling. *J. Neurosci.* **20,** 2835–2844
28. Valiunas, V. (2013) Cyclic nucleotide permeability through unopposed connexin hemichannels. *Front. Pharmacol.* **4,** 75
29. Ye, Z. C., Wyeth, M. S., Baltan-Tekkok, S., and Ransom, B. R. (2003) Functional hemichannels in astrocytes: a novel mechanism of glutamate release. *J. Neurosci.* **23,** 3588–3596
30. Hansen, D. B., Braunstein, T. H., Nielsen, M. S., and MacAulay, N. (2014) Distinct permeation profiles of the connexin 30 and 43 hemichannels. *FEBS Lett.* **588,** 1446–1457
31. Nielsen, M. S., Axelsen, L. N., Sorgen, P. L., Verma, V., Delmar, M., and Holstein-Rathlou, N. H. (2012) Gap junctions. *Compr. Physiol.* **2,** 1981–2035
32. Condorelli, D. F., Mudo, G., Barresi, V., and Belluardo, N. (2013) in *Gap Junctions in the Brain: Physiological and Pathological Roles* (Dere, E., ed) pp. 69–82, Academic Press, San Diego
33. Gosejacob, D., Dublin, P., Bedner, P., Hüttmann, K., Zhang, J., Tress, O., Willecke, K., Pfrieger, F., Steinhäuser, C., and Theis, M. (2011) Role of astroglial connexin30 in hippocampal gap junction coupling. *Glia* **59,** 511–519
34. Rash, J. E., Yasumura, T., Dudek, F. E., and Nagy, J. I. (2001) Cell-specific expression of connexins and evidence of restricted gap junctional coupling between glial cells and between neurons. *J. Neurosci.* **21,** 1983–2000
35. Wallraff, A., Köhling, R., Heinemann, U., Theis, M., Willecke, K., and Steinhäuser, C. (2006) The impact of astrocytic gap junctional coupling on potassium buffering in the hippocampus. *J. Neurosci.* **26,** 5438–5447
36. Harris, A. L. (2007) Connexin channel permeability to cytoplasmic molecules. *Prog. Biophys. Mol. Biol.* **94,** 120–143
37. Goldberg, G. S., Moreno, A. P., and Lampe, P. D. (2002) Gap junctions between cells expressing connexin 43 or 32 show inverse permselectivity to adenosine and ATP. *J. Biol. Chem.* **277,** 36725–36730
38. Weber, P. A., Chang, H. C., Spaeth, K. E., Nitsche, J. M., and Nicholson, B. J. (2004) The permeability of gap junction channels to probes of different size is dependent on connexin composition and permeant pore affinities. *Biophys. J.* **87,** 958–973
39. Schilling, W. P., Sinkins, W. G., and Estacion, M. (1999) Maitotoxin activates a nonselective cation channel and a P2Z/P2X(7)-like cytolytic pore in human skin fibroblasts. *Am. J. Physiol.* **277,** C755–C765
40. Browne, L. E., Compan, V., Bragg, L., and North, R. A. (2013) P2X7 receptor channels allow direct permeation of nanometer-sized dyes. *J. Neurosci.* **33,** 3557–3566
41. Yan, Z., Li, S., Liang, Z., Tomić, M., and Stojilkovic, S. S. (2008) The P2X7 receptor channel pore dilates under physiological ion conditions. *J. Gen. Physiol.* **132,** 563–573
42. Iglesias, R., Locovei, S., Roque, A., Alberto, A. P., Dahl, G., Spray, D. C., and Scemes, E. (2008) P2X7 receptor-Pannexin1 complex: pharmacology and signaling. *Am. J. Physiol. Cell Physiol.* **295,** C752–C760
43. Locovei, S., Scemes, E., Qiu, F., Spray, D. C., and Dahl, G. (2007) Pannexin1 is part of the pore forming unit of the P2X(7) receptor death complex. *FEBS Lett.* **581,** 483–488
44. Pelegrin, P., and Surprenant, A. (2006) Pannexin-1 mediates large pore formation and interleukin-1β release by the ATP-gated P2X7 receptor. *EMBO J.* **25,** 5071–5082
45. Moeller, H. B., Fenton, R. A., Zeuthen, T., and Macaulay, N. (2009) Vasopressin-dependent short-term regulation of aquaporin 4 expressed in *Xenopus* oocytes. *Neuroscience* **164,** 1674–1684
46. Ambrosi, C., Gassmann, O., Pranskevich, J. N., Boassa, D., Smock, A., Wang, J., Dahl, G., Steinem, C., and Sosinsky, G. E. (2010) Pannexin1 and Pannexin2 channels show quaternary similarities to connexons and different oligomerization numbers from each other. *J. Biol. Chem.* **285,** 24420–24431
47. Jespersen, T., Grunnet, M., Angelo, K., Klaerke, D. A., and Olesen, S. P. (2002) Dual-function vector for protein expression in both mammalian cells and *Xenopus laevis* oocytes. *BioTechniques* **32,** 536–538
48. Wiencken-Barger, A. E., Djukic, B., Casper, K. B., and McCarthy, K. D. (2007) A role for Connexin43 during neurodevelopment. *Glia* **55,** 675–686
49. Lippiat, J. D. (2008) Whole-cell recording using the perforated patch clamp technique. *Methods Mol. Biol.* **491,** 141–149

50. Sorensen, C. M., Salomonsson, M., Braunstein, T. H., Nielsen, M. S., and Holstein-Rathlou, N. H. (2008) Connexin mimetic peptides fail to inhibit vascular conducted calcium responses in renal arterioles. *Am. J. Physiol. Regul. Integr. Comp. Physiol.* **295,** R840–R847
51. Lai, C. P., Bechberger, J. F., Thompson, R. J., MacVicar, B. A., Bruzzone, R., and Naus, C. C. (2007) Tumor-suppressive effects of pannexin 1 in C6 glioma cells. *Cancer Res.* **67,** 1545–1554
52. Ramachandran, S., Xie, L. H., John, S. A., Subramaniam, S., and Lal, R. (2007) A novel role for connexin hemichannel in oxidative stress and smoking-induced cell injury. *PLoS One* **2,** e712
53. Contreras, J. E., Sánchez, H. A., Eugenin, E. A., Speidel, D., Theis, M., Willecke, K., Bukauskas, F. F., Bennett, M. V., and Sáez, J. C. (2002) Metabolic inhibition induces opening of unapposed connexin 43 gap junction hemichannels and reduces gap junctional communication in cortical astrocytes in culture. *Proc. Natl. Acad. Sci. U.S.A.* **99,** 495–500
54. De Bock, M., Wang, N., Bol, M., Decrock, E., Ponsaerts, R., Bultynck, G., Dupont, G., and Leybaert, L. (2012) Connexin 43 hemichannels contribute to cytoplasmic Ca^{2+} oscillations by providing a bimodal Ca^{2+}-dependent Ca^{2+} entry pathway. *J. Biol. Chem.* **287,** 12250–12266
55. De Vuyst, E., Decrock, E., Cabooter, L., Dubyak, G. R., Naus, C. C., Evans, W. H., and Leybaert, L. (2006) Intracellular calcium changes trigger connexin 32 hemichannel opening. *EMBO J.* **25,** 34–44
56. Clair, C., Combettes, L., Pierre, F., Sansonetti, P., and Tran Van Nhieu, G. (2008) Extracellular-loop peptide antibodies reveal a predominant hemichannel organization of connexins in polarized intestinal cells. *Exp. Cell Res.* **314,** 1250–1265
57. Schalper, K. A., Palacios-Prado, N., Retamal, M. A., Shoji, K. F., Martínez, A. D., and Sáez, J. C. (2008) Connexin hemichannel composition determines the FGF-1-induced membrane permeability and free $[Ca^{2+}]_i$ responses. *Mol. Biol. Cell* **19,** 3501–3513
58. Retamal, M. A., Froger, N., Palacios-Prado, N., Ezan, P., Sáez, P. J., Sáez, J. C., and Giaume, C. (2007) Cx43 hemichannels and gap junction channels in astrocytes are regulated oppositely by proinflammatory cytokines released from activated microglia. *J. Neurosci.* **27,** 13781–13792
59. Al-Ubaidi, M. R., White, T. W., Ripps, H., Poras, I., Avner, P., Gomès, D., and Bruzzone, R. (2000) Functional properties, developmental regulation, and chromosomal localization of murine connexin36, a gap-junctional protein expressed preferentially in retina and brain. *J. Neurosci. Res.* **59,** 813–826
60. Scemes, E., Bavamian, S., Charollais, A., Spray, D. C., and Meda, P. (2008) Lack of "hemichannel" activity in insulin-producing cells. *Cell Commun. Adhes.* **15,** 143–154
61. Srinivas, M., Rozental, R., Kojima, T., Dermietzel, R., Mehler, M., Condorelli, D. F., Kessler, J. A., and Spray, D. C. (1999) Functional properties of channels formed by the neuronal gap junction protein connexin36. *J. Neurosci.* **19,** 9848–9855
62. Charpantier, E., Cancela, J., and Meda, P. (2007) Beta cells preferentially exchange cationic molecules via connexin 36 gap junction channels. *Diabetologia* **50,** 2332–2341
63. Harris, A. L., and Locke, D. (2009) in *Connexins A Guide* (Harris, A. L., and Locke, D., eds) pp. 165–206, Humana Press Inc., Totowa, NJ
64. Yum, S. W., Zhang, J., Valiunas, V., Kanaporis, G., Brink, P. R., White, T. W., and Scherer, S. S. (2007) Human connexin26 and connexin30 form functional heteromeric and heterotypic channels. *Am. J. Physiol. Cell Physiol.* **293,** C1032–C1048
65. Kanaporis, G., Brink, P. R., and Valiunas, V. (2011) Gap junction permeability: selectivity for anionic and cationic probes. *Am. J. Physiol. Cell Physiol.* **300,** C600–C609
66. Unger, V. M., Kumar, N. M., Gilula, N. B., and Yeager, M. (1999) Three-dimensional structure of a recombinant gap junction membrane channel. *Science* **283,** 1176–1180
67. Maeda, S., Nakagawa, S., Suga, M., Yamashita, E., Oshima, A., Fujiyoshi, Y., and Tsukihara, T. (2009) Structure of the connexin 26 gap junction channel at 3.5 Å resolution. *Nature* **458,** 597–602
68. Oshima, A., Tani, K., Hiroaki, Y., Fujiyoshi, Y., and Sosinsky, G. E. (2007) Three-dimensional structure of a human connexin26 gap junction channel reveals a plug in the vestibule. *Proc. Natl. Acad. Sci. U.S.A.* **104,** 10034–10039
69. Stroud, R. M., Savage, D., Miercke, L. J., Lee, J. K., Khademi, S., and Harries, W. (2003) Selectivity and conductance among the glycerol and water conducting aquaporin family of channels. *FEBS Lett.* **555,** 79–84
70. Tsukaguchi, H., Shayakul, C., Berger, U. V., Mackenzie, B., Devidas, S., Guggino, W. B., van Hoek, A. N., and Hediger, M. A. (1998) Molecular characterization of a broad selectivity neutral solute channel. *J. Biol. Chem.* **273,** 24737–24743
71. MacVicar, B. A., and Thompson, R. J. (2010) Nonjunction functions of pannexin-1 channels. *Trends Neurosci.* **33,** 93–102
72. Suadicani, S. O., Iglesias, R., Wang, J., Dahl, G., Spray, D. C., and Scemes, E. (2012) ATP signaling is deficient in cultured Pannexin1-null mouse astrocytes. *Glia* **60,** 1106–1116
73. Bruzzone, R., Barbe, M. T., Jakob, N. J., and Monyer, H. (2005) Pharmacological properties of homomeric and heteromeric pannexin hemichannels expressed in *Xenopus* oocytes. *J. Neurochem.* **92,** 1033–1043
74. North, R. A. (2002) Molecular physiology of P2X receptors. *Physiol. Rev.* **82,** 1013–1067
75. Kubick, C., Schmalzing, G., and Markwardt, F. (2011) The effect of anions on the human P2X7 receptor. *Biochim. Biophys. Acta* **1808,** 2913–2922
76. Alberto, A. V., Faria, R. X., Couto, C. G., Ferreira, L. G., Souza, C. A., Teixeira, P. C., Fróes, M. M., and Alves, L. A. (2013) Is pannexin the pore associated with the P2X7 receptor? *Naunyn Schmiedebergs Arch. Pharmacol.* **386,** 775–787
77. Qiu, F., and Dahl, G. (2009) A permeant regulating its permeation pore: inhibition of pannexin 1 channels by ATP. *Am. J. Physiol. Cell Physiol.* **296,** C250–C255
78. Billaud, M., Lohman, A. W., Straub, A. C., Looft-Wilson, R., Johnstone, S. R., Araj, C. A., Best, A. K., Chekeni, F. B., Ravichandran, K. S., Penuela, S., Laird, D. W., and Isakson, B. E. (2011) Pannexin1 regulates α1-adrenergic receptor-mediated vasoconstriction. *Circ. Res.* **109,** 80–85
79. Weilinger, N. L., Tang, P. L., and Thompson, R. J. (2012) Anoxia-induced NMDA receptor activation opens pannexin channels via Src family kinases. *J. Neurosci.* **32,** 12579–12588
80. Figueroa, X. F., Lillo, M. A., Gaete, P. S., Riquelme, M. A., and Sáez, J. C. (2013) Diffusion of nitric oxide across cell membranes of the vascular wall requires specific connexin-based channels. *Neuropharmacology* **75,** 471–478
81. Orellana, J. A., Shoji, K. F., Abudara, V., Ezan, P., Amigou, E., Sáez, P. J., Jiang, J. X., Naus, C. C., Sáez, J. C., and Giaume, C. (2011) Amyloid β-induced death in neurons involves glial and neuronal hemichannels. *J. Neurosci.* **31,** 4962–4977
82. D'hondt, C., Ponsaerts, R., De Smedt, H., Bultynck, G., and Himpens, B. (2009) Pannexins, distant relatives of the connexin family with specific cellular functions? *BioEssays* **31,** 953–974
83. Wang, N., De Vuyst, E., Ponsaerts, R., Boengler, K., Palacios-Prado, N., Wauman, J., Lai, C. P., De Bock, M., Decrock, E., Bol, M., Vinken, M., Rogiers, V., Tavernier, J., Evans, W. H., Naus, C. C., Bukauskas, F. F., Sipido, K. R., Heusch, G., Schulz, R., Bultynck, G., and Leybaert, L. (2013) Selective inhibition of Cx43 hemichannels by Gap19 and its impact on myocardial ischemia/reperfusion injury. *Basic Res. Cardiol.* **108,** 309
84. Donnelly-Roberts, D. L., Namovic, M. T., Han, P., and Jarvis, M. F. (2009) Mammalian P2X7 receptor pharmacology: comparison of recombinant mouse, rat and human P2X7 receptors. *Br. J. Pharmacol.* **157,** 1203–1214
85. Ma, W., Hui, H., Pelegrin, P., and Surprenant, A. (2009) Pharmacological characterization of pannexin-1 currents expressed in mammalian cells. *J. Pharmacol. Exp. Ther.* **328,** 409–418
86. Marandykina, A., Palacios-Prado, N., Rimkutė, L., Skeberdis, V. A., and Bukauskas, F. F. (2013) Regulation of connexin36 gap junction channels by *n*-alkanols and arachidonic acid. *J. Physiol.* **591,** 2087–2101
87. Bhaskaracharya, A., Dao-Ung, P., Jalilian, I., Spildrejorde, M., Skarratt, K. K., Fuller, S. J., Sluyter, R., and Stokes, L. (2014) Probenecid blocks human P2X7 receptor-induced dye uptake via a pannexin-1 independent mechanism. *PLoS One* **9,** e93058
88. Stout, C. E., Costantin, J. L., Naus, C. C., and Charles, A. C. (2002) Intercellular calcium signaling in astrocytes via ATP release through connexin

hemichannels. *J. Biol. Chem.* **277,** 10482–10488
89. Hofer, A., and Dermietzel, R. (1998) Visualization and functional blocking of gap junction hemichannels (connexons) with antibodies against external loop domains in astrocytes. *Glia* **24,** 141–154
90. Morita, M., Saruta, C., Kozuka, N., Okubo, Y., Itakura, M., Takahashi, M., and Kudo, Y. (2007) Dual regulation of astrocyte gap junction hemichannels by growth factors and a pro-inflammatory cytokine via the mitogen-activated protein kinase cascade. *Glia* **55,** 508–515
91. Hofgaard, J. P., Mollerup, S., Holstein-Rathlou, N. H., and Nielsen, M. S. (2009) Quantification of gap junctional intercellular communication based on digital image analysis. *Am. J. Physiol. Regul. Integr. Comp. Physiol.* **297,** R243–R247